PHILOSOPHICAL TRANSACTIONS OF THE ROYAL SOCIETY A MATHEMATICAL, PHYSICAL & ENGINEERING SCIENCES

A Theoretical Analysis of the Use of Submarine Cables as Electromagnetic Oceanographic Flowmeters

I. S. Robinson

Phil. Trans. R. Soc. Lond. A 1976 **280**, 355-396
doi: 10.1098/rsta.1976.0002

A THEORETICAL ANALYSIS OF THE USE OF SUBMARINE CABLES AS ELECTROMAGNETIC OCEANOGRAPHIC FLOWMETERS

By I. S. ROBINSON

Institute of Oceanographic Sciences, Bidston Observatory, Birkenhead, Merseyside

(*Communicated by Sir George Deacon, F.R.S. – Received* 16 *December* 1974)

CONTENTS

An examination is made of the theoretical basis and simplifying assumptions governing the use of the voltage measured across the ends of a submarine cable as a measure of the sea flow across the cable section.

In part I a method of calculating the response of an electro-magnetic flowmeter by means of a weight vector is applied to the oceanographic situation. A numerical model is developed which generates the weight vector distribution for given submarine cables.

In part II, weight vector distributions are obtained for various cables around the British Isles, and the cable responses to given velocity distributions in the sea are calculated. It is shown that the velocity distributions associated with different tidal frequencies, storm surges and long period residual flows will result in different responses at a given cable. The implications of this are discussed. The effect on the cable response of seasonally varying sea conductivity, and of a tidal range which is not negligible compared with the mean depth, is also modelled.

I. THE THEORETICAL MODEL

1. Introduction

When sea water moves in the Earth's magnetic field, electromagnetic induction occurs in the electrically conducting fluid. Electric currents flow in the water, the sea bed and the surrounding land, so that the electric potential field which exists is determined by both the currents and the inductive effect. If the potential difference can be measured between two points in the sea, usually on opposite sides of a channel connected by a submarine telephone cable, the situation can be treated as a type of electromagnetic flowmeter, the measured potential difference being used as an indicator of the total volume transport of water through the channel at any instant. The system is calibrated by estimating the total flow from direct reading current measurements made at a few selected points in the channel over limited periods of time, from these obtaining the best constant of proportionality which satisfies the assumed linear relation between potential difference and volume transport, and using this same calibration constant over the much longer periods of time during which records have been obtained from the cable.

Such a system has been used in the Dover Straits by Bowden (1956) and Cartwright & Crease (1963), and in the Irish Sea by Bowden & Hughes (1961) and Hughes (1969). Submarine cables were also used by Wertheim (1954) to measure the transport in the Florida current between Havana and Key West. The method promises to be used regularly in the future since it is cheap to install and operate (given the existence of telephone cables) and can be a useful means of obtaining boundary data for real-time numerical sea models.

However, assumptions are made in the use of this method which may not always be justified. The analysis of the observations has been based on the work of Longuet-Higgins (1949), who explored the theory of electromagnetic induction in elliptical and rectangular section channels. His analysis was strictly for a channel of uniform cross section in the flow direction, with uniform conductivity in the sea. Some effects of variable sea conductivity were included in a more extended discussion of the problem by Longuet-Higgins, Stern & Stommel (1954). In practice, cables are often laid between two opposite headlands, at the narrowest part of a channel or between the mainland and an island, and the assumption of a straight, uniform channel is far from reality. Moreover, the conductivity of the sea may vary significantly over an area surrounding the cable. The assumption is made that these deviations from the theoretical conditions may be accounted for in the calibration procedure, i.e. although the sensitivity (potential difference/volume flow ratio) is not that predicted by theory it may be determined empirically. That is valid, in fact, only

if the sensitivity remains constant with time, and there are two reasons, at least, why this may not be so. (*a*) The velocity distribution in the channel may vary with time. If the velocity distribution does not significantly affect the sensitivity, then this is not a problem, as is the case in the effectively two dimensional analysis of Longuet-Higgins where the very large width/depth ratio eliminates the effect of any two dimensional flow distribution. Where the topography is more complex, with an irregularly shaped channel, local shallows, and varying conductivity, it is possible that different flow distributions will lead to different sensitivities, so that a tidally varying flow distribution will lead to a sensitivity varying with time. (*b*) The sensitivity is dependent upon the water depth unless the bed is insulating, and should there be a tidal range which is more than a small percentage of the mean depth, then again the system as an electromagnetic flowmeter exhibits a time-varying sensitivity. Neither can this be accounted for simply by introducing a time-varying depth into the Longuet-Higgins result and analysing the measured potentials accordingly, because the tide may vary in phase by a few hours over the area surrounding the cable. It should be noted that it is not just conditions at the section of channel between the two electrodes which contribute to the potential at the electrodes, but conditions over an area stretching upstream and downstream a distance of a few times the distance between the electrodes.

Thus it is clear that if measurement of volume flow by telephone cable potentials is to be reliable, especially to the extent of obtaining residual flow measurements, then we have to be confident that sensitivity is not varying with time. Each cable location must be taken on its own and evaluated for the influence which the above factors have on the sensitivity. It is the purpose of this paper to provide a way of modelling more accurately than hitherto more of the factors which contribute to the potential difference which is measured at a given cable location. By calculating the expected p.d. from typical velocity distributions and sea surface elevations during a tidal cycle, it should be possible to show whether the sensitivity varies to a significant extent or not. Information on conductivity, etc. is not sufficiently reliable (nor is modelling of the complex electrical resistance pattern of the sea bed sophisticated enough) to enable true values for sensitivity to be predicted. Empirical calibration would always be necessary, but a method is offered whereby a given cable situation may be tested to see whether it would lead to reliable, or virtually useless, estimates of water flow.

It should be emphasized that we are considering here only the flowmeter problem, and ignoring the electric field produced by the time-varying part of the Earth's magnetic field. None the less if the flowmeter effect can be realistically modelled, then it will be easier to subtract the contribution due to fluid motion from observations of electric field, thus giving a better estimate of the electric field which is linked to the time-varying magnetic field produced by ionospheric currents.

2. Basic theory

In recent years the theory of electromagnetic flow measurement has been significantly advanced by the work of Bevir (1970). Notably he developed the concept of a vector weighting function, the scalar product of which with the velocity at any point would give the contribution of that point to the total potential difference measured between the electrodes of the flowmeter. His work was applied specifically to pipe flowmeters with imposed magnetic fields. In this paper it is applied to the oceanographic flowmetering situation. The constraints of the real world are such in oceanography that Bevir's method cannot be applied to the design of an 'ideal meter', the rôle for which the weight function was first developed, but it can be used, as we have observed

PHILOSOPHICAL TRANSACTIONS OF THE ROYAL SOCIETY A MATHEMATICAL, PHYSICAL & ENGINEERING SCIENCES

above, for the modelling of a given situation to test for uniformity of sensitivity of the submarine cable used as a flowmetering device.

Within the water, the basic equations of magnetohydrodynamics apply, i.e. (Shercliff 1965)

	Ohm's law	$\boldsymbol{j} = \sigma(\boldsymbol{E} + \boldsymbol{v} \times \boldsymbol{B})$
	Kirchoff's first law	$\operatorname{div} \boldsymbol{j} = 0$
		$\operatorname{div} \boldsymbol{B} = 0$
	Ampère's law	$\operatorname{curl} \boldsymbol{B} = \mu \boldsymbol{j}$
and	Faraday's law	$\operatorname{curl} \boldsymbol{E} = -\partial \boldsymbol{B}/\partial t$

where $\boldsymbol{j}$ is electric current density, $\boldsymbol{E}$ is electric field strength, $\boldsymbol{B}$ is magnetic flux density, σ is electrical conductivity, μ is the magnetic permeability, t is time, and $\boldsymbol{v}$ is the fluid velocity.

Now if the magnetic Reynolds number ($\mu\sigma vd$) is small, as it is in sea water (d being a typical depth), the assumption can be made that Ampère's law be ignored, i.e. the magnetic field induced by induced currents is neglected compared with the imposed magnetic field (the Earth's field in this case). If we are to accommodate non-steady velocity flows into a quasi-static solution, then we must impose a further condition that any changes of electrical conditions due to a change of velocity diffuse throughout the relevant sea area in a time much less than a characteristic time of the velocity change. This is akin to the limitations of the skin effect in electrical engineering, and can be expressed for the oceanographic situation by requiring that a magnetic Reynolds number type of parameter, $\mu\sigma L\omega d \ll 1$, where ω is the frequency of velocity fluctuation and L is a horizontal length scale. It is appropriate for L to be the length of the cable. This expression is equivalent to equation (8.1.20) of Longuet-Higgins *et al.* (1954). In practice this means that for an M_2 tidal frequency $Ld \ll 1.4 \times 10^9\,\mathrm{m}^2$ and for M_4, $Ld \ll 4.7 \times 10^8\,\mathrm{m}^2$. A typical cable to be considered later is of length 100 km in sea of depth 100 m, which comfortably satisfies these criteria. If the sea bed is of comparable conductivity to the sea, d must include the depth of penetration of the induced currents, reducing the horizontal range of electrical diffusion. Given this quasi-static condition, we can assume that $\partial B/\partial t = 0$ and hence $\boldsymbol{E}$ may be represented as the gradient of a scalar, ϕ, the electric potential, i.e. $\boldsymbol{E} = -\nabla\phi$.

It may then be shown (Shercliff 1962) that $\nabla^2\phi = \operatorname{div}(\boldsymbol{v} \times \boldsymbol{B})$, which is the classical flowmeter equation, with σ uniform in the fluid. Applied to the oceanographic situation, this would have to be solved separately for each different velocity distribution encountered, and in the real sea, with non-uniform conductivity, the equation is more complex.

Bevir, however, makes use of the reciprocal relations that apply in electrical networks or continuous media, and for the general case of anisoptropic and non-uniform conductivity, proves that the potential difference between two electrodes in a fluid which moves through a magnetic field can be expressed as $U = \int \boldsymbol{v} \cdot \boldsymbol{W}\,\mathrm{d}\tau$. The volume integral is taken over the whole fluid space, and $\boldsymbol{W} = \boldsymbol{B} \times \nabla G$, where ∇G is a vector dependent only upon the shape of the flowmeter and electrodes, the conductivity of the fluid and the electrical boundary conditions at the walls. In our case this is therefore dependent only upon the topography and conductivity of the sea and bed. The form of ∇G is such that it is equivalent to the electrical current density distribution in the sea if unit current were injected at one electrode and extracted at the other, in the absence of $\sigma(\boldsymbol{v} \times \boldsymbol{B})$ currents. This 'virtual current' as Bevir terms it, bears no resemblance to the actual distribution of currents which flow due to the inductive effect of fluid motion, but is a purely mathematical concept which enables the potential difference to be calculated more easily in the above integral. The actual current distribution may well be extremely complex, but does not

need to be known. The problem of obtaining U for a given cable and given tidal flow thus resolves itself into that of calculating ∇G, the virtual current, for the given topography and conductivities of bed and sea, taking its vector product with $\boldsymbol{B}$, the scalar product of this with the velocity vector $\boldsymbol{v}$ at all points in the fluid, and finding the volume integral of this scalar product over the whole fluid volume. In practice, the integral is taken over a region in the vicinity of the cable, with checks to see that contributions to the integral at points around the boundary are minimal. It should be stressed that this form of solution of the flowmeter equation is not restricted to uniform conductivity of the fluid and bed, any variations of conductivity being accounted for in the calculation of ∇G. In what follows, Bevir's terminology of virtual current and virtual potential will be used to describe the weighting vector and its scalar potential, since it enables the solution for ∇G to be described in physical terms as a potential flow problem.

3. The solution for the virtual current in the oceanographic situation

Once the vector field ∇G is determined for a given cable situation, the response to any distribution of velocities is effectively characterized, assuming $\boldsymbol{B}$ is uniform and constant. In fact, the distribution of ∇G will give a good indication as to whether a cable is suitable for flowmetering or not, even before it has been used to find the response from different velocity distributions. Also, the variation of ∇G with different states of tidal elevation or different seasonal conductivities will give a good indication of the importance of these factors in affecting the sensitivity of the flowmeter.

Because of the complex three dimensional topography involved, an analytical solution for ∇G is not possible without the simplifications to a uniform section channel which have already been covered by Longuet-Higgins's theory. The advantage of using the virtual current method is that it can readily be adapted to a numerical solution for each individual case. To assist the solution, some reasonable assumptions can be made, while still leaving the problem flexible enough to cope with the factors mentioned in § 1 which have hitherto been ignored in submarine cable analysis.

(*a*) *Thin slab assumption*

The sea may be treated as a thin slab of varying thickness, the assumption then being possible that virtual current density is not dependent upon depth, in the sea itself. This is realistic in view of the very large length/depth ratios involved in the continental shelf waters, of order 100–1000, any variation of virtual current in the vertical direction being smoothed out in a horizontal distance comparable to the sea depth, i.e. negligible compared with the horizontal scales of the topography. Thus the virtual current in the sea itself may be modelled in a two dimensional horizontal grid.

(*b*) *The electrodes*

These may be modelled as current inputs to the squares in which they occur. In practice, a finite length of the submarine cable earth sheathing acts as the electrode, in electrical contact with both sea bed and adjacent sea water, but the effective length is not likely to exceed the dimensions of the grid square, i.e. of the order of 1 km. If it does, then the use of the cable sheathing as an electrode is questionable, since it is effectively shorting out the signal from those portions of the total flow occurring close inshore, and other electrodes should be used.

PHILOSOPHICAL TRANSACTIONS OF THE ROYAL SOCIETY A MATHEMATICAL, PHYSICAL & ENGINEERING SCIENCES

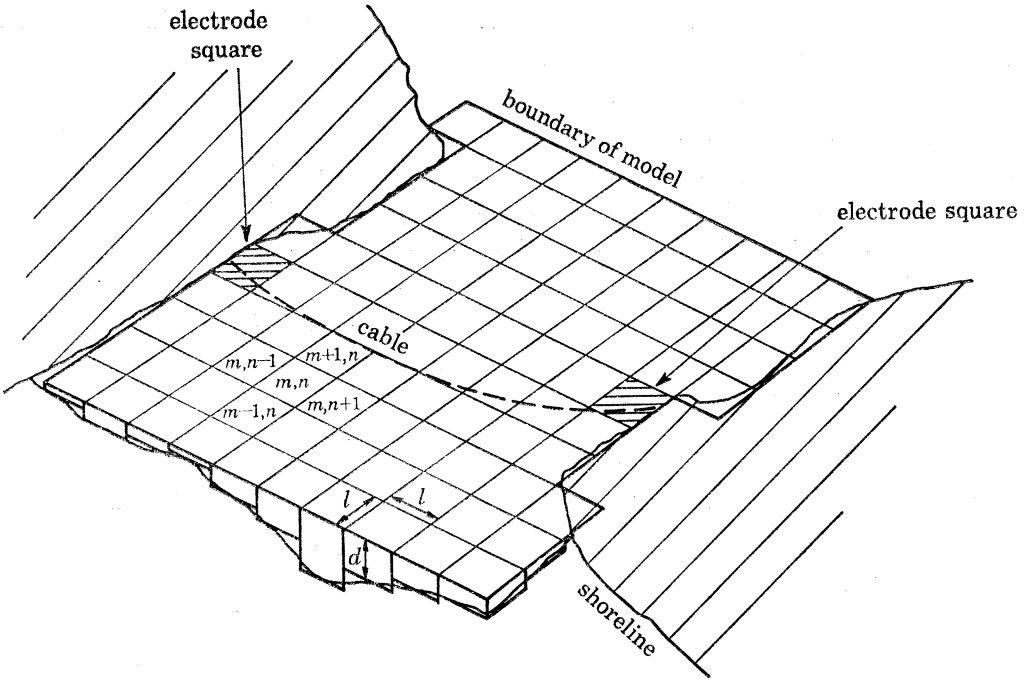

FIGURE 1. Arrangement of virtual current model grid.

Thus the simple model is as shown in figure 1. The area of sea is divided into squares of side l. The sea conductivity and depth d are defined in each square. The virtual electric potential $V_{m,n}$ is defined at the centre of square m, n and the virtual current passing from one square to the next, $I_{m,n}$ and $J_{m,n}$ are defined at the points shown in figure 2. If the sea bed were insulating, this simple model would suffice to define ∇G, but with a conducting bed, account must be taken of the virtual current which passes through the bed and does not contribute to W within the fluid. The modelling of the earth virtual currents is dealt with in the next section, and to allow for the earth currents, $K_{m,n}$ is defined as the current passing from the sea to the earth in grid square m, n.

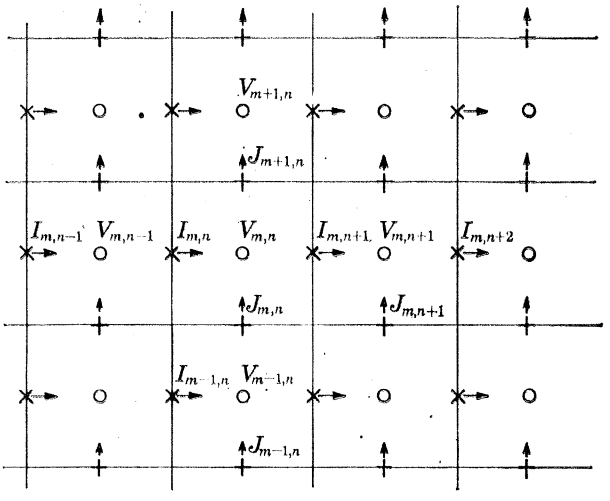

FIGURE 2. Detail of grid notation.

Then the equations in finite difference form are

$$\text{div}\,\boldsymbol{j} = 0 \text{ leads to: } I_{m,n} + J_{m,n} = I_{m,n+1} + J_{m+1,n} + K_{m,n} \text{ for each square;} \tag{1}$$

curl $\boldsymbol{E} = 0$ has already been assumed in that a virtual electric potential V has been defined. Ohm's law ($\boldsymbol{j} = \sigma \boldsymbol{E} = -\sigma \nabla \phi$) leads to $I_{m,n}/dl = \sigma(V_{m,n-1} - V_{m,n})/l$, d and σ being defined at the virtual current grid points, i.e.

$$I_{m,n} = b_{m,n}(V_{m,n-1} - V_{m,n}), \tag{2}$$

and in the perpendicular direction

$$J_{m,n} = c_{m,n}(V_{m-1,n} - V_{m,n}), \tag{3}$$

where

$$\begin{aligned} b_{m,n} &= \tfrac{1}{2}(d_{m,n}\sigma_{m,n} + d_{m,n-1}\sigma_{m,n-1}), \\ c_{m,n} &= \tfrac{1}{2}(d_{m,n}\sigma_{m,n} + d_{m-1,n}\sigma_{m-1,n}), \end{aligned} \tag{4}$$

i.e. the values of $d\sigma$ at the current points have been taken as the average of the $d_{m,n}\sigma_{m,n}$ defined in the adjacent squares.

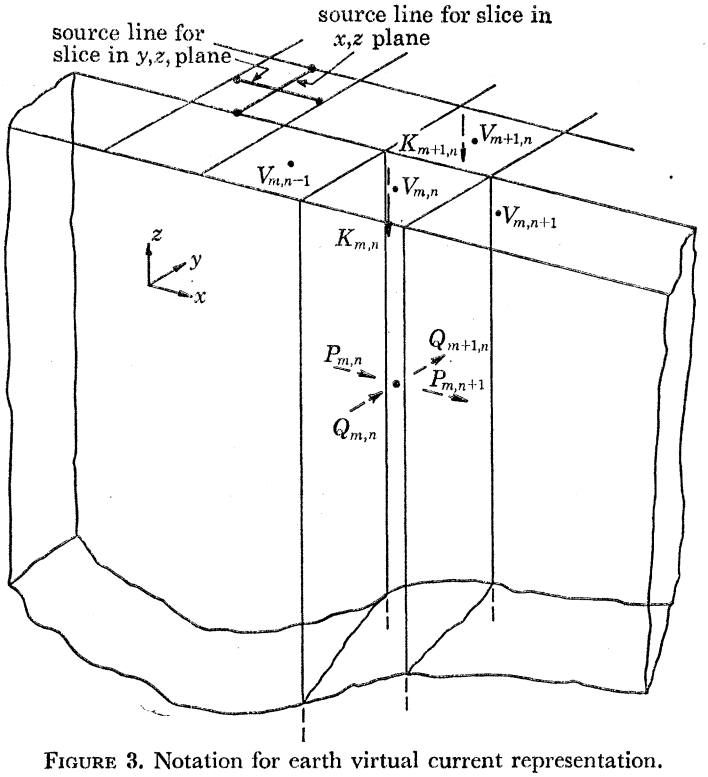

FIGURE 3. Notation for earth virtual current representation.

4. EARTH VIRTUAL CURRENT DISTRIBUTION

To solve equations (1) and (3) for $I_{m,n}$ and $J_{m,n}$ it is necessary to know $K_{m,n}$, the total virtual current lost to earth in each grid square, which means that it is necessary to solve for the virtual current distribution in the earth. Since we are concerned only with the total virtual earth current passing beneath a given grid line, and not the virtual current density dependence on the vertical coordinate, it is expedient to reduce the problem to one of two dimensions whereby the sum $P_{m,n}$ and $Q_{m,n}$ of the virtual current crossing the semi-infinite strips reaching vertically downwards beneath the grid lines, is related to the virtual electric potential distribution at the sea/sea

bed interface, i.e. the distribution of potential in the simple slab model above (see figure 3). This relation is approximately modelled as follows:

Consider a vertical slice of earth, the faces running beneath two adjacent grid lines from one boundary of the modelled area to the opposite boundary, as shown in figure 3. Given the limitations of the finite difference approximation, the virtual potential must be considered as invariant in the direction normal to the faces of the slice, within each individual slice, so that we can now consider the two dimensional distribution of virtual current in the plane of the slab faces, i.e. the planes containing the vertical and one of the horizontal dimensions. This can be modelled in terms of the superposition of virtual current line sources and sinks of strength P_r per unit length which become point sources of strength P_r in the two dimensional representation of figure 4. This assumes that all the current $K_{m,n}$ entering or leaving the earth in a grid square does so through the two perpendicular source or sink lines in that square (corresponding to the two perpendicular slices passing beneath that square). While not physically realistic, this assumption is satisfactory within the limits of the finite difference approximation and leads to a more tractable mathematical solution than the other possible assumption of uniformly distributed current inflow across the grid square, which leads to a singularity of potential gradient at the grid lines. Another definite approximation implicit in this approach is that within each slice the two dimensional divergence is zero. This is not generally true but the presence of the sources and sinks at the surface is intended to accommodate the transfer of current to adjacent slices which in fact occurs throughout the whole area of the slice.

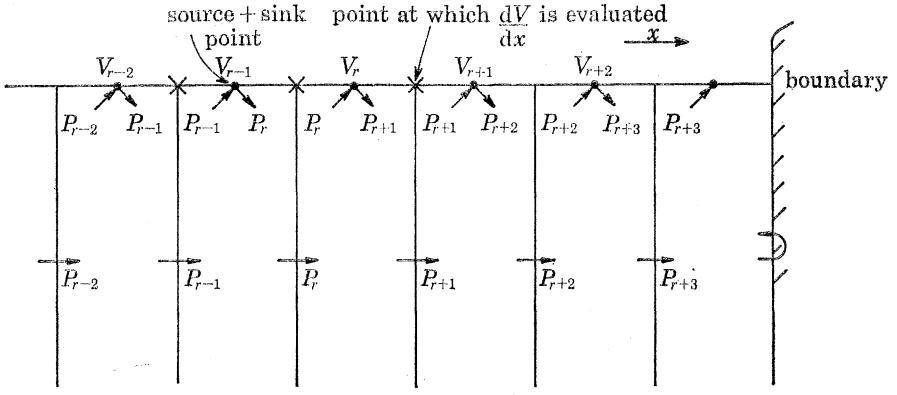

FIGURE 4. Source–sink arrangement to represent earth virtual current distribution.

By inspection of figure 4 it can be seen that if sources and sinks are arranged in pairs as shown, the total current crossing beneath the surface grid lines within the slice is equal to the strength of the source and sink pair which straddles the line in question, i.e. we have equated lP_r to $P_{m,n}$ or $Q_{m,n}$. The problem then becomes that of obtaining the electric field strength or potential gradient at the grid points in terms of the strengths of the sources and sinks.

Consider the complex plane $\zeta = x + iy$. Let the potential function $F(\zeta) = -\sigma_E \phi + i\psi$, where ϕ represents the electric potential, ψ the electric current stream function and σ_E the conductivity of the Earth (assumed uniform). Then the potential due to a source of strength $2P_r$ at a position $x = +b$ on the y axis is $F = 2P_r \ln(x + iy - b)$. This models the potential in the semi-infinite plane with a source of strength P_r at $x = b$, $y = 0$ and zero current flow across $y = 0$. Then

$$-\sigma_E \phi = \mathrm{Re}\,(F(z)) = P_r \ln((x-b)^2 + y^2).$$

Hence $$\frac{\partial\phi}{\partial x} = -\frac{2P_r(x-b)}{\sigma_E((x-b)^2+y^2)}.$$

Now if the origin be taken at the grid line on the surface, at that point $(\partial\phi/\partial x)_{x=0,y=0} = 2P_r/\sigma_E b$. Now in the slice of figure 4,

$$P_r = \pm\frac{P_{m,n+k}}{l}, \quad b = \tfrac{1}{2}l(2k \mp 1).$$

Hence $$\left(\frac{\partial\phi}{\partial x}\right)_{m,n} = \frac{8}{\sigma_E l^2}\Sigma\frac{P_{m,n+k}}{4k^2-1},$$

the summation taken over k such that all $P_{m,n}$ are included from row m of the grid. Thus

$$V_{m,n} - V_{m,n-1} = \frac{8}{\sigma_E l}\Sigma\frac{P_{m,n+k}}{4k^2-1}, \tag{5}$$

$$V_{m,n} - V_{m-1,n} = \frac{8}{\sigma_E l}\Sigma\frac{Q_{m+k,n}}{4k^2-1}. \tag{6}$$

The continuity equation for earth currents is

$$P_{m,n} + Q_{m,n} + K_{m,n} = P_{m,n+1} + Q_{m+1,n}. \tag{7}$$

Substituting equations (1), (2), (3) in (7), we have

$$\begin{aligned} b_{m,n}(V_{m,n-1} - V_{m,n}) + c_{m,n}(V_{m-1,n} - V_{m,n}) + P_{m,n} + Q_{m,n} \\ = P_{m,n+1} + Q_{m+1,n} + b_{m,n+1}(V_{m,n} - V_{m,n+1}) + c_{m+1,n}(V_{m,n} - V_{m+1,n}). \end{aligned} \tag{8}$$

Equations (5), (6) and (8) are the finite difference equations for numerical solution.

5. Boundary conditions

The sea boundary conditions are that round the limits of the area considered, there is zero virtual current outflow through each square, i.e. the equation (1) will have only three terms in I and J, or two at corner squares, with the corresponding effect in equation (8). This boundary condition also implies that V should be constant along an open sea boundary, and how closely the calculated result approaches this condition will be an indication of whether the modelled area is sufficiently large. This in turn will indicate the area of sea which contributes to the measured signal at the submarine cable.

At the two electrode squares, where the virtual current source and sink are considered to be, there will be an additional term of $+1$ and -1 respectively on the left hand side of equation (8). However, of the set of continuity equations (8), one is redundant, since if the external inputs and outputs to the system balance and if the currents J and I satisfy continuity in all but one square, they must automatically satisfy it in the last one. To provide the necessary extra equation to enable solution, the absolute value of the potential must be fixed in one square, e.g. the sink square, and may arbitrarily be chosen as zero. Thus, $V_{m,n} = 0$ replaces the continuity equation for that square in the set (8).

The earth virtual current boundary conditions involve the approximation, for simplicity, that the net virtual current flow below grid square sides at the boundary is zero. This is justified since all the virtual current which flows out from the system will flow back into the modelled area at a different depth, and most of it probably below the same grid square. Since the earth currents

PHILOSOPHICAL TRANSACTIONS OF THE ROYAL SOCIETY A MATHEMATICAL, PHYSICAL & ENGINEERING SCIENCES

are likely to be a small percentage of the sea currents, it was not considered worth while to model this boundary condition any more accurately. The exception is where a headland protrudes into the sea, and the sea model boundary follows the coast. In this case earth currents can jump across the headland which is represented by an 'earth-only' grid square and adjustments must be made to the set of equations (5), (6) and (8).

6. Computer method to evaluate virtual current

A numerical model was constructed in which equations (5), (6) and (8) could be solved by a digital computer. The grid squares of figures 1 and 2 are indexed both by a one dimensional sequence and by their position in the two dimensional array defining their position in space. Hence adjacent squares can be located through the two dimensional array, but not every square in the two dimensional grid need be filled, and rows and columns can be of arbitrary lengths, with gaps if necessary, thus providing sufficient versatility for the model to be applied to any cable situation with only a change in input data necessary. Information is input for each square regarding the average sea depth, sea conductivity, and whether the square has an east, west, north or south boundary with the limits of the model or with an earth-only square where such are deemed necessary to allow for the flow of current through a headland or island.

Since it is assumed that the proportion of the virtual current passing through the earth will be somewhat less than that through the sea, an iterative procedure is used to solve for V. The series of equations (8) for all the sea squares can be represented in a matrix equation

$$\mathbf{A}\mathbf{v} = \mathbf{b}.$$

$\mathbf{A}$ is composed of terms in $b_{m,n}$ and $c_{m,n}$, and $\mathbf{b}$ consists of terms containing P and Q, except for the row in the equations corresponding to the sink square s for which $V = 0$, whence

$$a_{st} = 0, \quad a_{ss} = 1, \quad b_s = 0.$$

Now,

$$\mathbf{v} = \mathbf{A}^{-1}\mathbf{b},$$

and because $\mathbf{A}$ is not altered during the iteration process, it is necessary to invert it once only. $\mathbf{A}$ can be up to a size of 200×200, and inversion is performed numerically by the standard Gauss–Jordan method. A check is included to test for numerical accuracy of such a large inversion. Initially $\mathbf{b}$ is set to zero except for a value of -1 corresponding to the source square. Consequently the first solution for V corresponds to that with zero earth conductivity. At this stage, values of V in the earth-only squares are supplied, being taken simply as the mean of the V values of adjacent sea squares. P and Q are then obtained from equations (5) and (6), again using a matrix inversion technique, i.e.

$$\mathbf{G}\mathbf{p} = \mathbf{h}$$

applies to each row or column of the two dimensional model grid. $\mathbf{G}$ is composed of terms from the summations in (5) and (6) and $\mathbf{h}$ is formed from the V terms, including the earth-only squares.

Now,

$$\mathbf{p} = \mathbf{G}^{-1}\mathbf{h},$$

the inversion having to be performed for each row or column since $\mathbf{G}$ changes with different lengths of rows or columns. Should there be any blank squares (i.e. outside the limits of the model boundary) sandwiched between model squares within a row or column, these are included in the setting up of $\mathbf{G}$, but do not affect the result since $\mathbf{h}$ is set with zero value for those squares.

The values of P and Q so obtained are used to form new values for $\boldsymbol{b}$, whence $\boldsymbol{v}$ is once more calculated to give a new set of V taking earth currents into account. However, it is necessary to scale the values of P and Q before insertion into $\boldsymbol{b}$ so that the model does not become unstable. This is done by calculating the sea currents in each square from the values of V, and considering the total current I_t, in both sea and earth, crossing the perpendicular bisector of the line joining the source and sink squares, across the whole width of the model. Now since all the current passing from source to sink crosses this line, I_t should equal unity when the model is producing the correct solution. If $I_t > 1$, then the calculated earth currents are too large, and if $I_t < 1$ they are too small. Consequently P and Q are scaled by the factor $(I_t)^{-1}$ before insertion into $\boldsymbol{b}$.

The process is repeated, using the values of P and Q obtained from the previous iteration to calculate V and hence new values of P and Q, until successive iterations produce negligible change in the value of V. As a test, a parameter r is calculated, which is the root mean square value of the net currents flowing into each square through both sea and land (after removing the unit input and output at the source and sink squares), and this should tend to zero if the solution is converging. Its failure to converge on zero is a measure of the limits of numerical accuracy which are possible. In the earth-only squares, the constraints of the model do not automatically require the net current inflow to be zero, and so the magnitude of r in these cases is also a measure of the error involved in the arbitrary assignment of mean values of V to these squares.

Provided the solution converges, and is sufficiently accurate, the two components of virtual current are calculated at the centre of each sea square from the mean of the respective component values at the sides of the square as computed from V. These results characterize the response of the cable, and are output on cards for use with different velocity distributions in the calculation of the theoretical voltage produced by a given flow pattern. This is achieved in a simple program which performs the sum $\Sigma B_V(\nabla G \times \boldsymbol{v})$, B_V being the vertical component of the Earth's magnetic field, assumed constant, and $\boldsymbol{v}$ the sea velocity defined in every sea square of the model, the summation being taken over all the sea squares. It is necessary also to multiply by the length of a grid square to obtain the true volume integral and end up with units of volts.

7. Example to illustrate the computer model

The use of the model can be illustrated by its application to the cable between Port Erin on the Isle of Man and Cemaes Bay on Anglesey. The grid which was initially adopted for this cable is shown in figure 5. Three land-only squares are used to represent those parts of the Isle of Man near the cable end which could contribute significantly to the distribution of virtual current, and one such square was used on Anglesey. Depths for each grid square were obtained from Admiralty Chart No. 1824a. The sea conductivity was calculated in each square by using the U.S. Navy tables (Bialek 1966), from mean temperature and salinity distributions given by Bowden (1955) for August. The earth conductivity, of necessity assumed uniform, was taken to be $0.015\,\mathrm{S\,m^{-1}}$, midway between the estimates made by Bowden & Hughes (1961) for the North Channel and for St George's Channel from an analysis of cable measurements using Longuet-Higgins's formula for a straight uniform channel. Although this value cannot be considered very reliable, it does at least give an order of magnitude estimate for σ_E.

Figure 6 shows the resulting virtual current distribution, represented in magnitude and direction by the lines whose centre is the centre of a grid square. As might be expected, the greatest contribution comes from those sea areas closest to the cable ends. It will also be noted that the

PHILOSOPHICAL TRANSACTIONS OF THE ROYAL SOCIETY A MATHEMATICAL, PHYSICAL & ENGINEERING SCIENCES

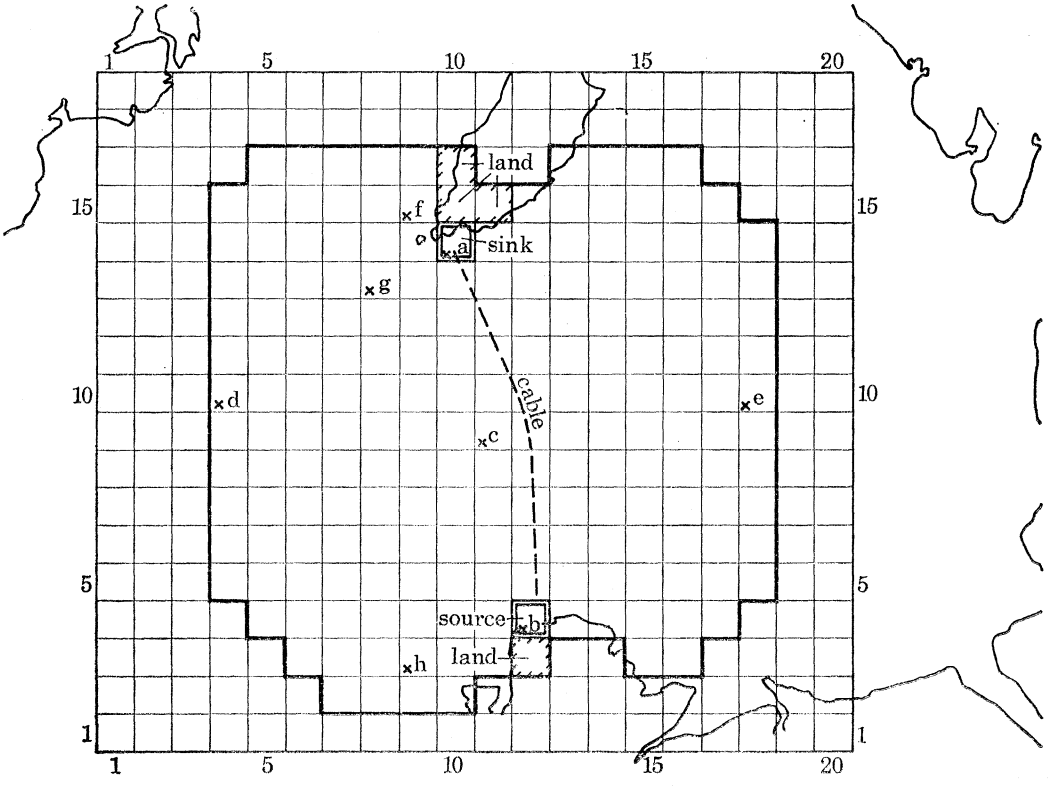

FIGURE 5. Grid for first model of Castletown–Cemaes Bay cable.
×, Sample squares used in figure 8*b*.

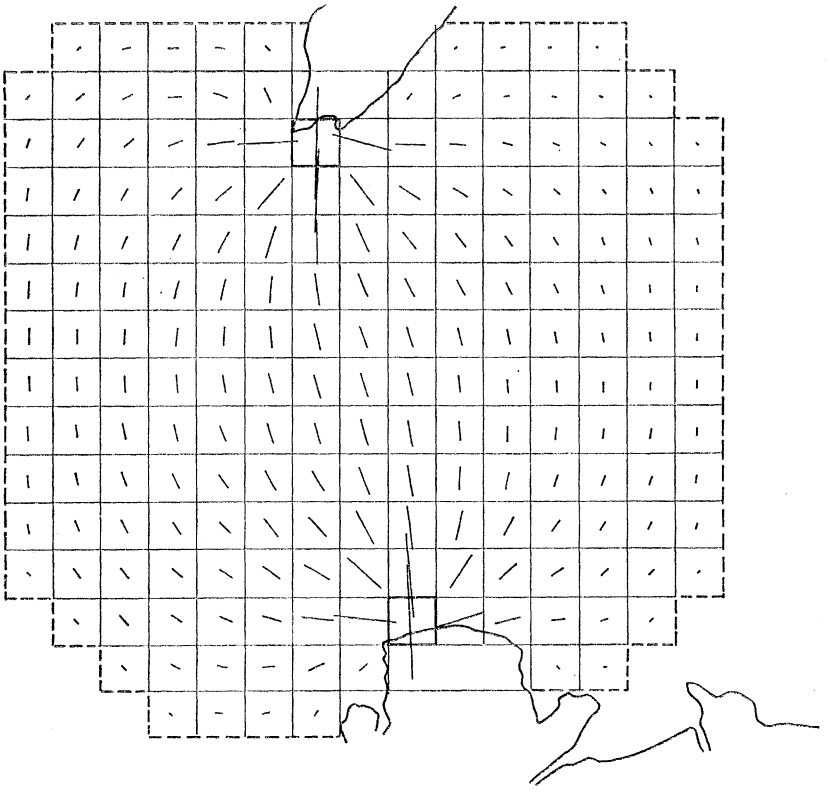

FIGURE 6. Virtual current distribution from Castletown–Cemaes Bay cable, model 1.

PHILOSOPHICAL TRANSACTIONS OF THE ROYAL SOCIETY A MATHEMATICAL, PHYSICAL & ENGINEERING SCIENCES

vectors at the western boundary where the sea is deepest are nearly half the magnitude of those in the centre of the model, indicating that this model is not extensive enough to cover that area of sea which makes a significant contribution to the voltage signal picked up by the ends of the cable. A more satisfactory model of larger area was used for further study of the effect of different flow patterns, and will be described in a later section.

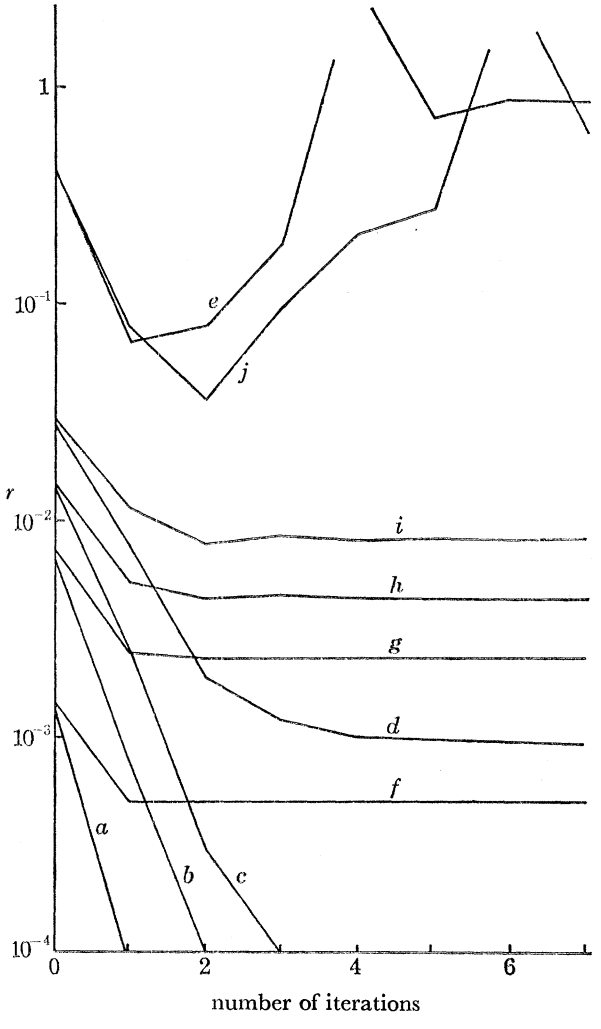

FIGURE 7. Convergence characteristics of Cemaes Bay–Castletown cable model 1. (r is the root mean square of the net currents flowing into each square.) (a) $\sigma_E = 0.0015$ S m^{-1}; (b) 0.0075; (c) 0.015; (d) 0.030; (e) 0.15. ((a)–(e), land squares excluded from model.) (f) $\sigma_E = 0.0015$ S m^{-1}; (g) 0.0075; (h) 0.015; (i) 0.030; (j) 0.15. ((f)–(j), land squares included in the model.)

However, this initial grid was used to give some indications of the reliability of the model. In particular the modelling of the virtual current through the earth could possibly give rise to errors in three ways: (i) even assuming it is fairly uniform, the estimated value of σ_E may be significantly wrong, (ii) the theoretical representation of the earth currents is rather crude, and (iii) continuity of virtual current is denied by estimating the virtual potential in the earth-only squares. Hence the model was run with and without the land squares included for five different values of earth conductivity centred about the estimates of 0.015. Attention was paid to the convergence of the numerical method, the ratio of virtual current in the sea to that in the earth, which would

influence the theoretical calibration of the cable, and the distribution of the virtual current throughout the sea, which would influence the variation of response of the cable to different flow distributions. The convergence characteristics are shown in figure 7, where r is plotted against the number of iterations of the numerical process, for the different runs. The programme was stopped after seven iterations. It will be seen that convergence occurred after four iterations for all except the highest earth conductivity at which an initial convergence gave way to increasing and oscillating values of r. On closer inspection of the results, the divergence was seen to result from those grid squares where scaling of the earth currents by $(I_t)^{-1}$ before entering them into the vector $\boldsymbol{b}$ was not sufficient to prevent a local instability, which gradually spread throughout the model. In subsequent models of other cables, when the estimated earth conductivity was such as to cause a similar situation, it was found to be possible to obtain convergence by scaling the earth currents in the first few iterations by a factor $(2I_t)^{-1}$. The introduction of earth-only squares did not appear to affect whether convergence occurred or not, but did result in a convergence to a non-zero value of r, which increased with σ_E.

Figure 8*a* gives an indication of the relative proportions of virtual current in the sea and earth, being the sum of the virtual currents crossing the perpendicular bisector of the cable in the sea, and in the earth, plotted against σ_E. It will be noted that their sum, which should be unity, is greater than one when earth-only squares are included in the model, indicating the extent of the continuity inconsistency introduced by estimating the virtual potential in those squares. The theoretical calibration for each case was calculated using an M_2 tidal velocity distribution produced by a numerical model of Mungall, as described in the next section, and is plotted in figure 8 also. Clearly the estimate of σ_E is crucial if the cable is to be calibrated by this theoretical model alone. On the other hand, if the cable has been previously calibrated empirically with some confidence, then a curve such as figure 8 can furnish a reliable estimate of σ_E. This dependence on σ_E is not a serious drawback because the fundamental purpose of the model was not to give an actual calibration, but to determine the variation of sensitivity due to different flow profiles. The effect of σ_E on this variation may be gauged by considering the relative distribution in space of the virtual current in the sea. A measure of this can be obtained by taking the virtual current at the sample points indicated in figure 5, and normalizing them by dividing by the total sea current crossing the perpendicular bisector of the cable. The results are plotted in figure 8*b*. It can be seen that in general, the effect of increasing σ_E is to increase the weighting towards the cable ends. However, this is not so dependent upon the estimate of σ_E as the calibration was, in that an order of magnitude increase of σ_E will only increase the end weighting by about 20 %. The use of land squares appears to influence the distribution only in the immediate vicinity of the squares concerned.

The conclusions to be drawn from this checking of the effect of σ_E are that it is hazardous to attempt a calibration of the cable by theoretical means alone if σ_E is not known reliably, but provided the right order of magnitude is estimated for σ_E, the shape of the virtual current distribution, and hence the ability to predict the dependence of the cable sensitivity on different flow patterns, can be obtained with some confidence. If σ_E can be estimated by matching a theoretically predicted tidal calibration with an empirical calibration then this confidence can be increased. It is also concluded that unless there are headlands or islands close to the cable ends where the virtual current is large, it would be best not to include earth-only squares in the model because of the errors they introduce.

It is worth while here to briefly examine the virtual current distribution of figure 6, to illustrate

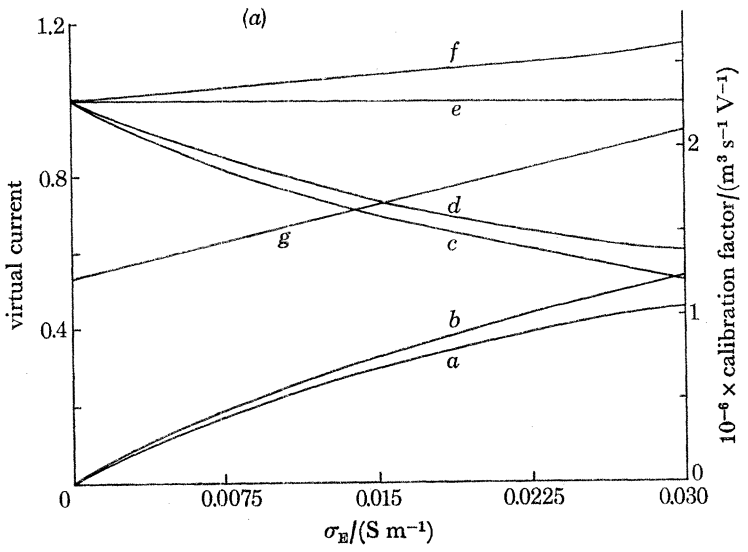

FIGURE 8 (*a*). Variation of virtual current distribution between sea and earth, and of calibration factor, with earth conductivity. (*a*) Total virtual current passing through sea bed across centre of model, land squares excluded from model. (*b*) Total virtual current passing through sea bed across centre of model, land squares included in model. (*c*) Total virtual current passing through sea across centre of model, land squares excluded from model. (*d*) Total virtual current passing through sea across centre of model, land squares included in model. (*e*) (*a*) + (*c*). (*f*) (*b*) + (*d*). (*g*) Calibration factor.

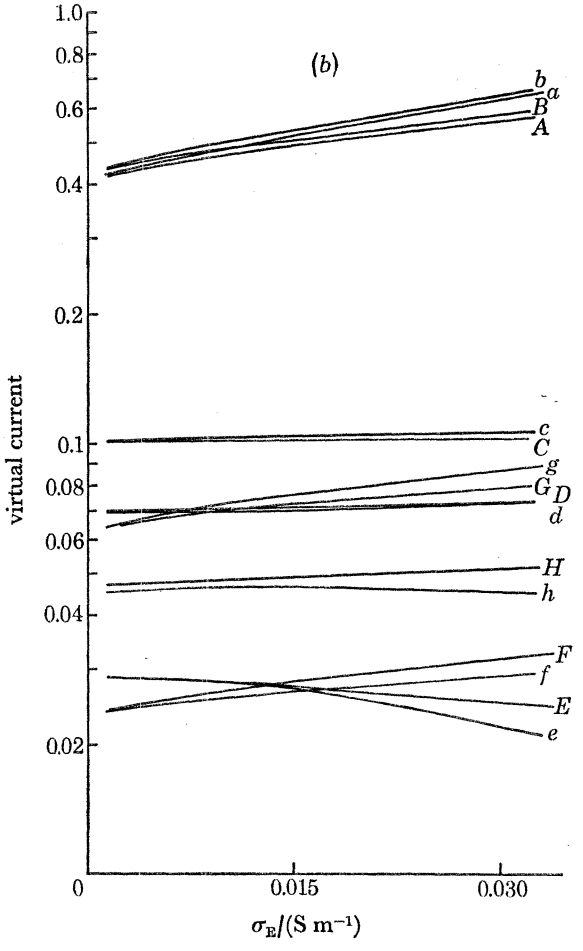

FIGURE 8 (*b*). Virtual current in sample squares, variation with earth conductivity. The squares are defined in figure 5. The lower case letters denote the results from a model with land-only squares excluded, and capitals the results from a model including them. (*a–e*) North–south components; (*f–h*) East–west components.

what implications can be drawn from it regarding the response of the cable to different flow situations. The clearest way of demonstrating that the sensitivity will not be the same in all cases is to consider two flows, each having the same volume transport across the cable section, but one of uniform flow distribution and the other having the flow concentrated in the centre of the channel, dropping to zero at the coasts. The weighting of the virtual current vector towards the cable ends means that the latter case will produce a voltage signal which is less than for the former case, and the sensitivity will be correspondingly less. If in the course of a tidal cycle, or the duration of a storm surge, the flow pattern varied between these two possibilities, then the cable sensitivity would vary in time. Another illustration is to consider a tidal flow of progressive wave type. Because the virtual current tends to be greater in the western half than in the eastern half of the model, then if the wave progresses from west to east the voltage signal will reach its maximum ahead of the transport across the cable section reaching its maximum, i.e. the signal will have a phase lead relative to the volume transport to which it is supposed to bear a non-complex linear dependence. On the other hand if the wave progresses east to west there will be a phase lag. A third flow situation that could be envisaged is where there are strong currents from the south-west flowing northwards to the west of Anglesey, such as to cause a signal to be picked up by the cable, while in fact there is zero transport through the channel between the Isle of Man and Anglesey. In the rest of the paper actual situations around the British Isles will be considered to determine whether such effects as these are of sufficient importance to impair the use of the cables as reliable flowmeters.

Figure 6 can also give some indication of the probable effect of conductivity variation. Seasonal changes in conductivity occurring over the whole area are more likely to affect the overall proportion of earth virtual current to sea virtual current rather than the actual distribution pattern in the sea. However, a local time-varying non-uniformity of conductivity, such as a tidal variation due to the flushing of a brackish estuary or a diurnal effect due to solar heating of shallow water, will have the effect of distorting the current pattern with consequent effect on the tidal voltage signal. This will be worst when such non-uniformities occur close to the cable ends.

II. SPECIFIC APPLICATIONS OF THE MODEL

8. General considerations

Having developed a model for calculating the theoretical voltage signal to be expected from a given flow distribution, we shall now analyse specific applications of the model in different cable situations. Because the submarine cable is not an 'ideal' flowmeter – i.e. one which has the same sensitivity to all flow distributions – it is always possible to invent a particular hypothetical velocity pattern which would give nonsensical cable-voltage results. However, what really matters is whether the cable copes adequately with the actual flow-measuring tasks it is required to perform. We shall therefore aim to restrict the tests we impose to flow patterns which are realistic. Because the model is likely to be sensitive to flow patterns which are not self-consistent (e.g. which do not obey continuity considerations) it is best to introduce current distributions which are output from realistic numerical dynamical models of tides and surges, and therefore self-consistent. With this in mind the virtual current models in the Irish Sea have been designed with grids to match dynamical Irish Sea models, which facilitates the handling of the velocity data. Where no numerical model exists, the tidal stream atlases have been used to provide an estimate of the velocity distribution.

PHILOSOPHICAL TRANSACTIONS OF THE ROYAL SOCIETY A MATHEMATICAL, PHYSICAL & ENGINEERING SCIENCES

Rather than investigate all the characteristics of individual cables, particular cables have been used to illustrate general points having universal application. Thus the Dover cable has been used particularly to investigate the effect that the variation of depth due to tidal rise and fall has on the cable sensitivity, since the Dover Strait is a place where the tidal range is not insignificant in relation to the depth. Because the Irish Sea gives a large seasonal range of sea conductivity, the effect of this on the seasonal variation of cable sensitivity has been studied using the Anglesey – Isle of Man cable as an illustration. The Irish Sea also has a fairly complex topography, and so various Irish Sea cables have been used to study (i) the cable signal for a single harmonic (M_2) and the comparison of the resulting calibration with the empirical calibration, (ii) the variation of response to different tidal harmonics and consequent distortion of the tidal curve, and (iii) the response of the cables to typical storm surges and wind-driven circulations, to decide whether calibrations based on the dominant tidal motions can be applied to convert voltage residuals into true residual volume transports.

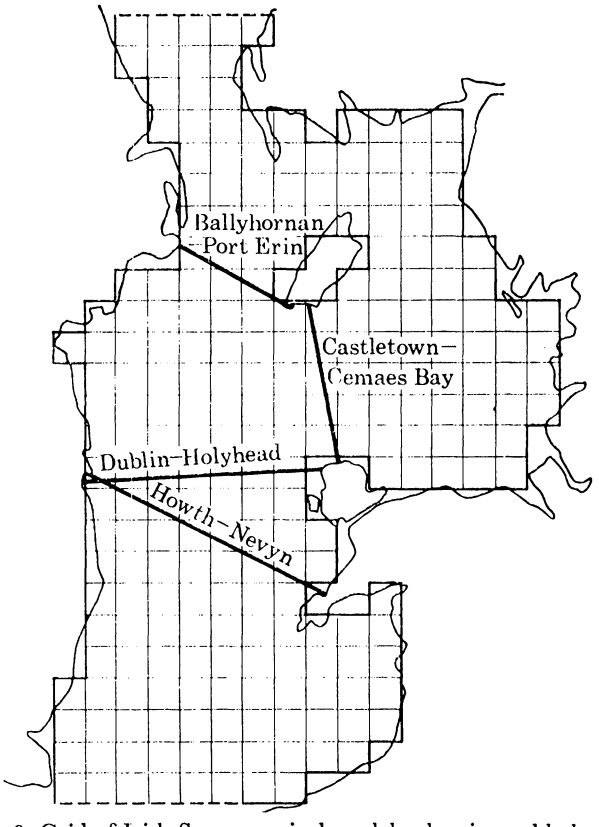

FIGURE 9. Grid of Irish Sea numerical models, showing cable locations.

9. THE RESPONSE OF THE IRISH SEA CABLES TO A SINGLE (M_2) TIDAL HARMONIC

The dominant signal from any cable around the British Isles is the M_2 semi-diurnal frequency, which consequently is the basis of empirical cable calibrations. Accordingly, the response of four Irish Sea cables to a pure M_2 velocity distribution was calculated by the virtual current method. The cables chosen were those from Cemaes Bay (Anglesey) to Castletown (Isle of Man), Ballyhornan (N. Ireland) to Port Erin (Isle of Man), Holyhead to Dublin and Nevin to Howth.

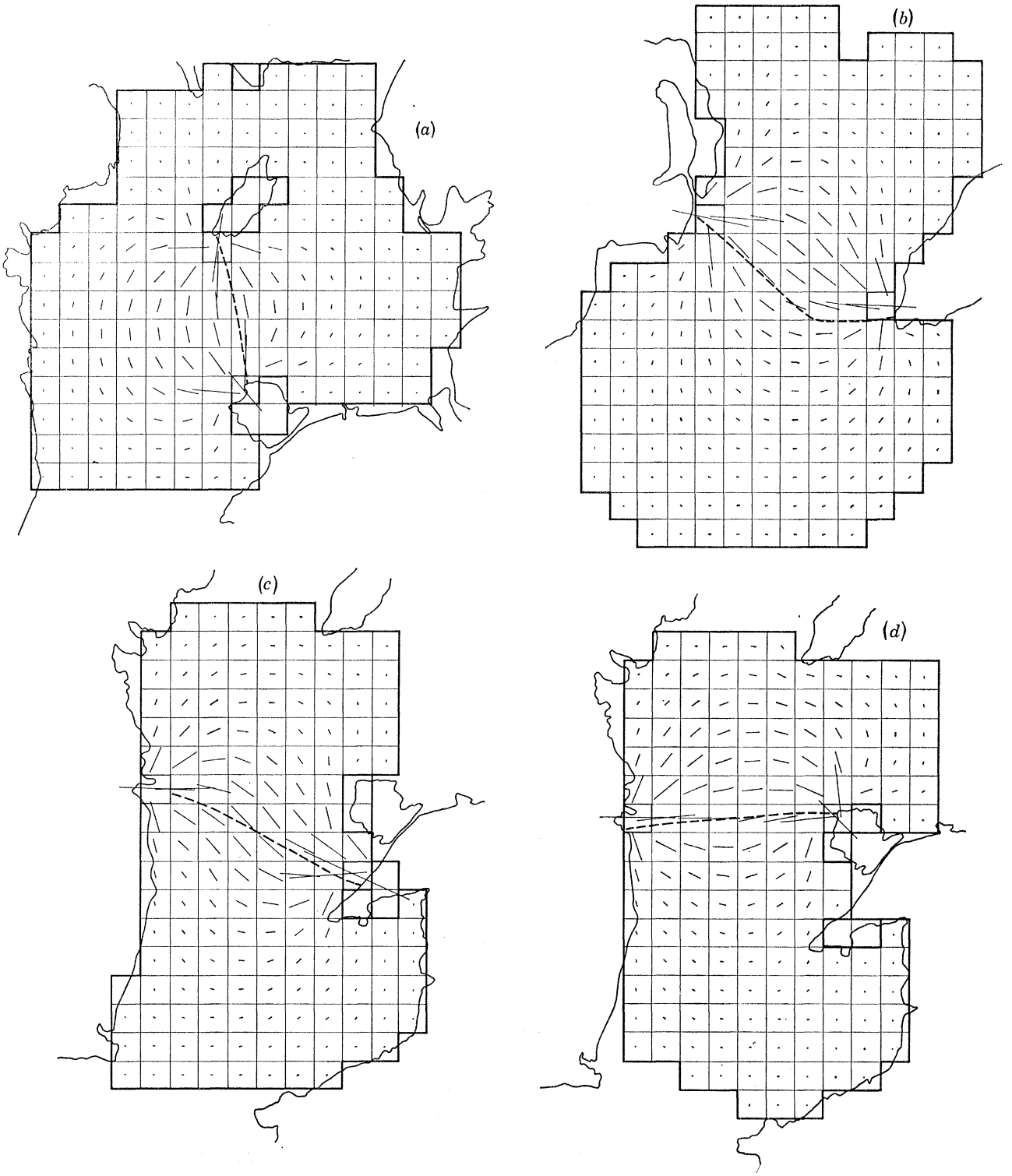

FIGURE 10. The grids used for, and virtual current distributions obtained from the Irish Sea cable models. (*a*) Cemaes Bay–Castletown cable, model 2, grid square size = 13.9 km. (*b*) Port Erin–Ballyhornan cable, grid square size = 6.95 km. (*c*) Nevyn–Howth cable, grid square size = 13.9 km. (*d*) Holyhead–Dublin cable, grid square size = 13.9 km. Heavily outlined squares not containing a vector are land squares. The heavily outlined squares at the cable ends are source and sink squares.

PHILOSOPHICAL TRANSACTIONS OF THE ROYAL SOCIETY A MATHEMATICAL, PHYSICAL & ENGINEERING SCIENCES

The choice of these cables was made because they all lie well within the boundaries of various dynamical models of the Irish Sea developed by the I.O.S. Bidston modelling group. The virtual current grid for each cable model was chosen to coincide with the grid for the dynamical models which is shown in figure 9, with the location of each cable. Figures 10*a–d* show the limits of the areas modelled for each individual cable, with details of land squares and the virtual current source and sink squares. The calculated virtual current is represented in magnitude and direction by the line vectors in each grid square. The model operated by using depths obtained from Admiralty Chart 1824a, and sea conductivities defined for each square from the mean August distributions of temperature and salinity given by Bowden (1955). The earth conductivities (see table 1) were those deduced by Bowden & Hughes (1961) from the analysis of empirical cable results using Longuet-Higgins' formula. The M_2 velocities were obtained from the results of a dynamical tidal model, with M_2 input at the boundaries, developed by Mungall (1973). The amplitude and phase at each grid square were supplied, enabling the volume transport across the cable section and the expected voltage signal to be calculated at 15° phase intervals through a tidal cycle. Since the operations to calculate these results are both linear, the input of a purely M_2 velocity distribution results in a purely M_2 output. There is, however, a phase shift which depends upon the spatial distribution of the phase of the velocity. This is apparent when the volume transport and voltage signal are plotted over a tidal cycle (figure 11*a–d*). The phase agreement is remarkably good, particularly for the Nevin–Howth and Holyhead–Dublin cables which pass close to the degenerate amphidromic region off Southern Ireland where the M_2 phases change rapidly in space and might be expected to influence the phase of the voltage. Due to the phase shift, the ratio of volume transport to voltage signal (also plotted in figure 11), has a singularity. The true amplitude ratio may be obtained from the ratio of the peaks, and it is this which represents the calibration of the cable. Table 1 lists the calibration of each cable, comparing this theoretical value with the calibrations made empirically and reported in the literature.

TABLE 1. IRISH SEA CABLE PARAMETERS AND CALIBRATIONS

					theoretical calibration			
cable	$10^3\sigma_E$ / S m^{-1}	cross-sect. area / km^2	channel width / km	mean depth / m	transport / 10^6 m^{3}s^{-1}V^{-1}	depth mean velocity / ms^{-1}V^{-1}	phase lag (voltage behind transport) / deg	empirical transport calibration / 10^6 m^{3}s^{-1}V^{-1}
Cemaes Bay–Castletown	15.0	3.87	73.9	52.4	1.63	0.42	−1.3	1.95 (Hughes)
Port Erin–Ballyhornan	15.0	3.84	56.8	67.6	1.86	0.48	4.5	1.47 (Hughes)
Howth–Nevyn	8.5	7.59	104.2	72.8	2.08	0.25	−3.0	3.80 (2.97) (Bowden & Hughes)
Holyhead–Dublin	8.5	6.45	102.0	63.3	1.87	0.29	−4.5	—

The two cables to the Isle of Man give quite close agreement between empirical and theoretical calibrations, the difference being around 20 % of the theoretical value. For the Anglesey cable the theoretical calibration is lower than the empirical, and vice versa for the N. Ireland cable. By the reasoning of § 7 these differences could be eliminated by varying the earth conductivity by less than a factor of 2. If incorrect earth conductivity is the cause of the discrepancy,

it is not sufficiently in error to mean that the virtual current distribution (and hence the theoretical cable response to varying velocity distributions) is unrealistic. It is, however, quite possible that some of the difference could be accounted for by inaccuracy of the empirical calibration. The calculation of volume transport across a section from current measurements at isolated stations is open to errors. If the theoretical analysis could be supplied with a true value of earth con-

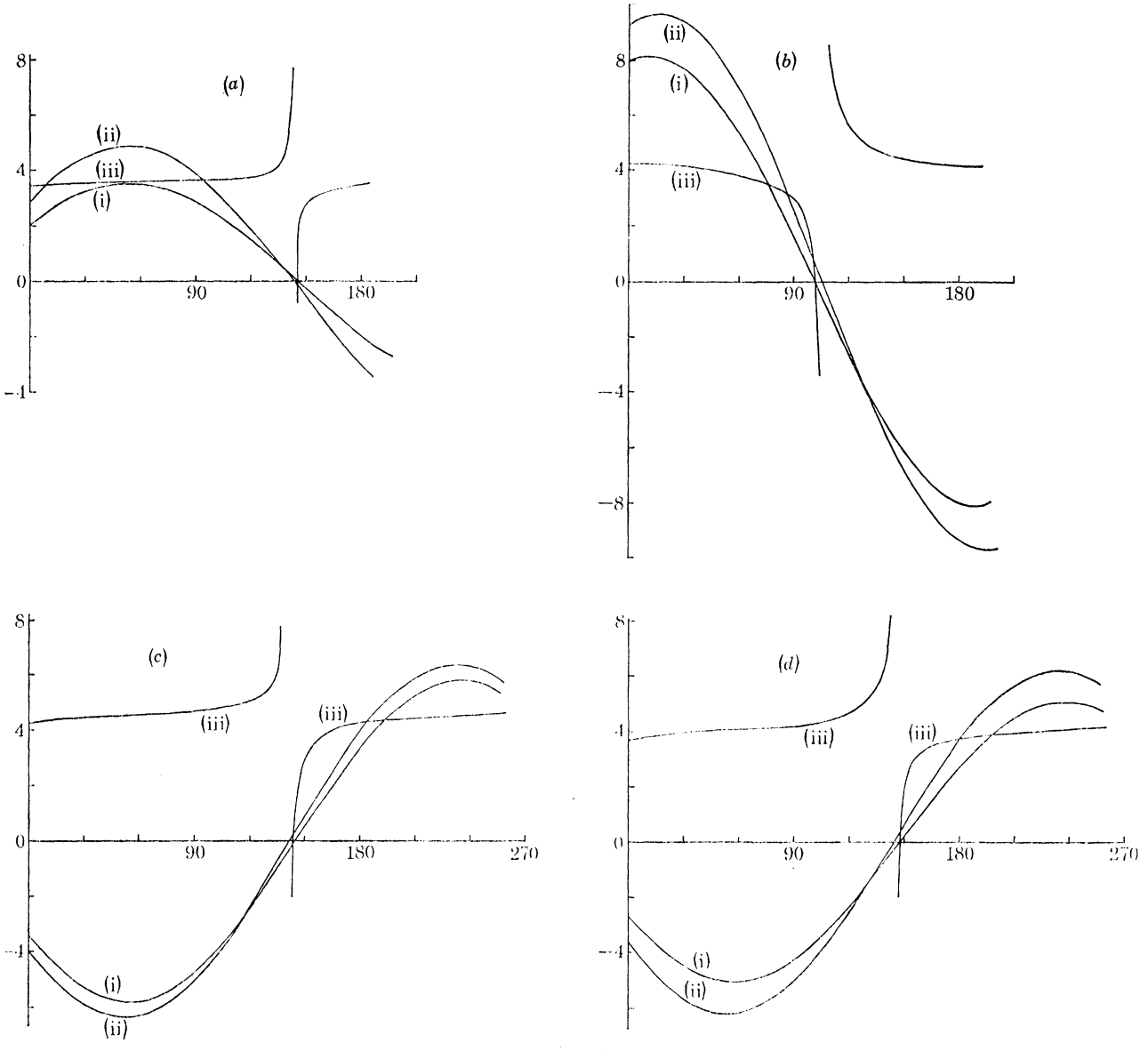

FIGURE 11. Theoretical cable response to a pure M_2 input velocity, over half a tidal cycle. (*a*) Cemaes Bay–Castletown cable: curve (i) volume transport, one unit is 10^6 m^3 s^{-1}; (ii) voltage signal, one unit is 0.44 V; (iii) instantaneous calibration, one unit is 4.55×10^5 m^3 s^{-1} V^{-1}. (*b*) Port Erin–Ballyhornan cable: curve (i) volume transport, one unit is 10^5 m^3 s^{-1}; (ii) voltage signal, one unit is 4.4×10^{-2} V; (iii) instantaneous calibration, one unit is 2.27×10^5 m^3 s^{-1} V^{-1}. (*c*) Nevyn–Howth cable: curve (i) volume transport, one unit is 10^6 m^3 s^{-1}; (ii) voltage signal, one unit is 0.44 V; (iii) instantaneous calibration, one unit is 4.55×10^5 m^3 s^{-1} V^{-1}. (*d*) Holyhead–Dublin cable: curve (i) volume transport, one unit is 10^6 m^3 s^{-1}; (ii) voltage signal, one unit is 0.44 V; (iii) instantaneous calibration, one unit is 4.55×10^5 m^3 s^{-1} V^{-1}.

ductivity, and the empirical calibration could use a dynamical model to deduce volume transport more accurately from isolated current and elevation values, then the two approaches could be compared more meaningfully. Given the limitations of both approaches, the present results are considered to be satisfactory, and to indicate that the theoretical 'virtual current' approach is modelling reality quite closely.

No empirical calibration could be found for the Dublin–Holyhead cable. A simple analysis taking Longuet-Higgins' formula (i.e. e.m.f. $\propto$ velocity $\times$ length of cable), ignoring earth currents, suggests that the depth mean velocity calibration should be inversely proportional to cable length, and the volume transport calibration proportional to the mean depth. On that basis, comparing the Nevin–Howth and the Holyhead–Dublin cables with the two Isle of Man cables makes the theoretical value seem very reasonable. Hughes (personal communication) gives an empirical calibration of the Nevin–Howth cable (correcting a typographical error in the value of $1.062\,\mathrm{m\,s^{-1}\,V^{-1}}$ quoted by Bowden & Hughes (1961)), of $0.50\,\mathrm{m\,s^{-1}\,V^{-1}}$ for the depth mean current, which gives $3.80\times10^{6}\,\mathrm{m^{3}\,s^{-1}\,V^{-1}}$ for the volume transport. He also points out that more recent current meter measurements have led to a calibration factor of $2.97\times10^{6}\,\mathrm{m^{3}\,s^{-1}\,V^{-1}}$. While the theoretical value of $2.08\times10^{6}\,\mathrm{m^{3}\,s^{-1}\,V^{-1}}$ is sufficiently close to the empirical to make its use in the following sections meaningful, there is nevertheless a significant difference to account for. This may in part be due to the errors of empirical measurement, but probably suggests that the earth conductivity used in the calculations is too low, resulting in too high a theoretical voltage. At $8.5\times10^{-3}\,\mathrm{S\,m^{-1}}$, σ_{E} is based on the figure deduced by Bowden & Hughes using Longuet-Higgins formula and the empirical calibration, but it is half the value used for the other Irish Sea cables.

The calibrations calculated in this section will be taken as the standard calibration for the interpretation of any voltages obtained using the virtual current distributions which are derived here.

10. The effect of seasonally varying sea conductivity

As the conductivity of sea water changes due to seasonal temperature and salinity changes, so the sensitivity of the cable varies. This has been observed in practice by taking the monthly mean M_2 range of voltage signals on the Dover cable (Bowden 1956; Cartwright & Crease 1963) and the Irish Sea cables (Hughes 1969). From the point of view of the present approach, this can be explained in terms of the proportion of virtual current passing through the sea relative to that through the sea bed. As the sea conductivity increases, more virtual current passes through the sea, resulting in higher voltages registered by the cable due to a given velocity distribution. If the sea bed were insulating, all the virtual current would pass through the sea anyway, and consequently variation of sea conductivity would not affect the cable sensitivity. The extent to which seasonal variation of sea conductivity affects the cable calibration is therefore dependent upon the value of earth conductivity.

To test the ability of the present method to model this seasonal variation, the Cemaes Bay–Castletown model was supplied with sea conductivity data derived from Bowden (1955), for February, May and November, as well as for the August values used above. The mean value of conductivity ranged from around $3.0\,\mathrm{S\,m^{-1}}$ in February to $4.0\,\mathrm{S\,m^{-1}}$ in August. The resulting virtual current distributions were then used with the M_2 tidal velocities of Mungall, as above, to produce curves of expected voltage over a tidal cycle. It was found that the phase lag of voltage relative to volume transport did not vary more than 0.25° across the seasons. The amplitude

varied more noticeably, however, being greatest in August and least in February as expected. Table 2 lists the different values of cable calibration. In figure 12 the voltage output has been scaled to have an annual mean range of 27.5 units, to enable comparison with the empirical results recorded by Hughes (1969) for this cable. As can be seen, the seasonal variation predicted by the model is some 30 % smaller than that observed in 1965, and considerably less than the 1964 observations. Now it has already been noted above that the theoretical (August) calibration of this cable is lower than Hughes's empirical value. This of itself cannot account for the discrepancy in seasonal variation since the seasonal variation has already been scaled proportionately to the mean value. However, it may indicate that the earth conductivity has been underestimated,

TABLE 2. SEASONAL VARIATION OF CALIBRATION
(CEMAES BAY–CASTLETOWN CABLE)

earth conductivity in model / S m^{-1}	month	mean sea conductivity / S m^{-1}	cable calibration / 10^6 m^3 s^{-1} V^{-1}
0.015	February	3.35	1.68
	May	3.60	1.665
	August	4.10	1.63
	November	3.80	1.65
0.0225	February	3.35	2.66
	May	3.60	2.58
	August	4.10	2.42
	November	3.80	2.51

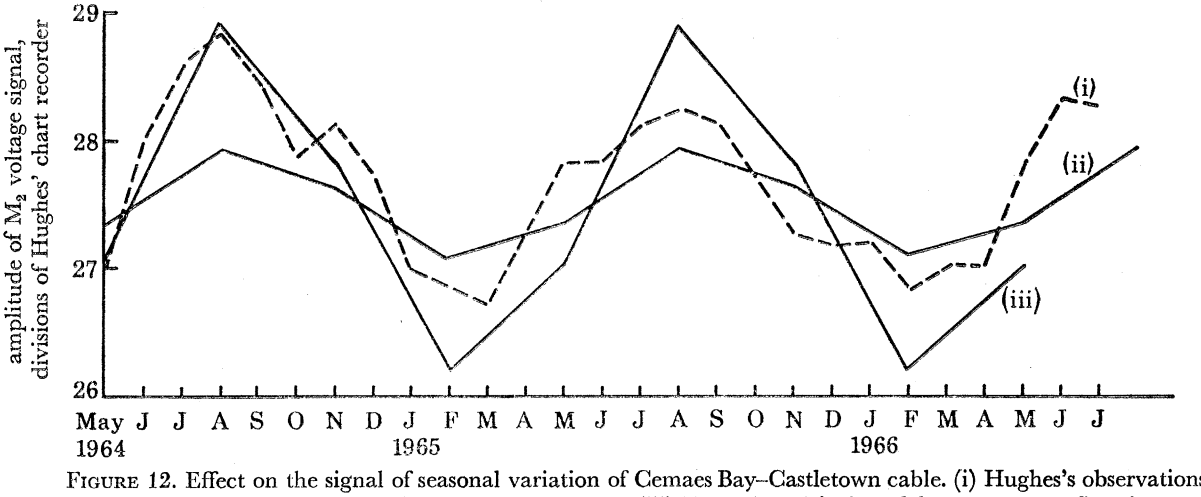

FIGURE 12. Effect on the signal of seasonal variation of Cemaes Bay–Castletown cable. (i) Hughes's observations. (ii) From theoretical model, $\sigma_E = 0.015$ S m^{-1}. (iii) From theoretical model, $\sigma_E = 0.0225$ S m^{-1}.

which could also contribute to this reduction of seasonal variation. By using figure 8 as a guide (although it is for a different model of the same cable), a σ_E of 0.0255 S m^{-1} should give a calibration approximately the same as the empirical value. This was tried for the four seasons, and the resulting calibrations are given in table 2 and plotted on figure 12. The seasonal variation of the model is now as large as the 1964 observed variations, and if anything is too large. The corresponding calibration factor is also too large, suggesting that σ_E has now been overestimated. However, it is evident that the seasonal variation of calibration can be closely modelled, and can be used as a check on the accuracy of estimating σ_E.

It must be noted that the seasonal variation of cable response is due not only to the variation of the mean sea conductivity, but also to the variation of distribution of conductivity in space from season to season. Hence in a region where the tidal phase varied considerably in space, the phase lag also might be expected to change seasonally. In § 12 mention will be made of the seasonal variation of the cable response to a wind-driven circulation pattern, as a measure of this effect of spatial variation of conductivity with season.

11. The response to a spectrum of tidal frequencies

It was pointed out in § 9 that because the lunar semi-diurnal frequency dominates the cable records it is the basis of cable calibration. In all work making use of cable voltages the assumption is made, tacitly if not explicitly, that the M_2 calibration can be applied to all other tidal frequencies and any mean or residual flows. While this assumption greatly simplifies the empirical calibration of a cable, and if true extends its usefulness, it is not necessarily valid since the response of the cable is dependent on the flow distribution in the sea, which may vary from harmonic to harmonic. In particular it will vary between different tidal species, as a comparison between the cotidal charts for different species will readily show. Harmonics of the same species tend to have a broadly similar distribution of cotidal lines, whereas those of different species can have a completely different pattern. Consequently a different calibration might be expected to be appropriate for a different species. Hughes' comparison between the Holyhead tide-gauge levels and the voltage from the Cemaes Bay–Port Erin cable show similar amplitude ratios for the semi-diurnal frequencies but very different ratios for some of the diurnal and quarter-diurnal frequencies, which tends to bear this out. Of course the diurnal cable frequencies may well be influenced by earth currents, and it may be inaccurate to equate quarter-diurnal period elevations with the velocity through the section. Using the present method it is now possible to test whether the variation of calibration between different species is significant or not. Given an accurate knowledge of diurnal tidal current distribution it might be possible to accurately separate the sea-generated diurnal voltages from the measured to give the voltage due to diurnal earth-generated currents.

It was also noted above that the cable response involves both an amplitude ratio and a phase lag between voltage signal and volume transport. Hence it is necessary to evaluate the complex cable response, ideally over all tidal frequencies, if a proper picture of a cable's characteristics is to be obtained. In the present work, using the cable models described in § 9, no velocity input was available from a numerical model containing all tidal frequencies. However, depth mean velocities were obtained from a tidal model of the Irish Sea developed by Banks (J. E. Banks, private communication). This has M_2 input at the sea boundaries, and because it is a non-linear model, when it has reached a steady state it contains the mean flow and higher harmonics of M_2 which result from non-linear operations on M_2. Twenty-five half-hourly values of current at each of the sea squares were used to evaluate the cable voltage over a tidal cycle for each of the four Irish Sea cables. This voltage is scaled by the calibration factors derived in § 9, to represent cable-based estimates of volume transport which can be compared with the actual volume transport. The results are shown in figure 13. M_2 dominates the results, and it is hard to distinguish from this to what extent other harmonics are truly represented by the cable voltage. The plot of instantaneous calibration (i.e. volume transport/voltage at each half-hourly interval) follows a similar shape to that for M_2 only in figure 11.

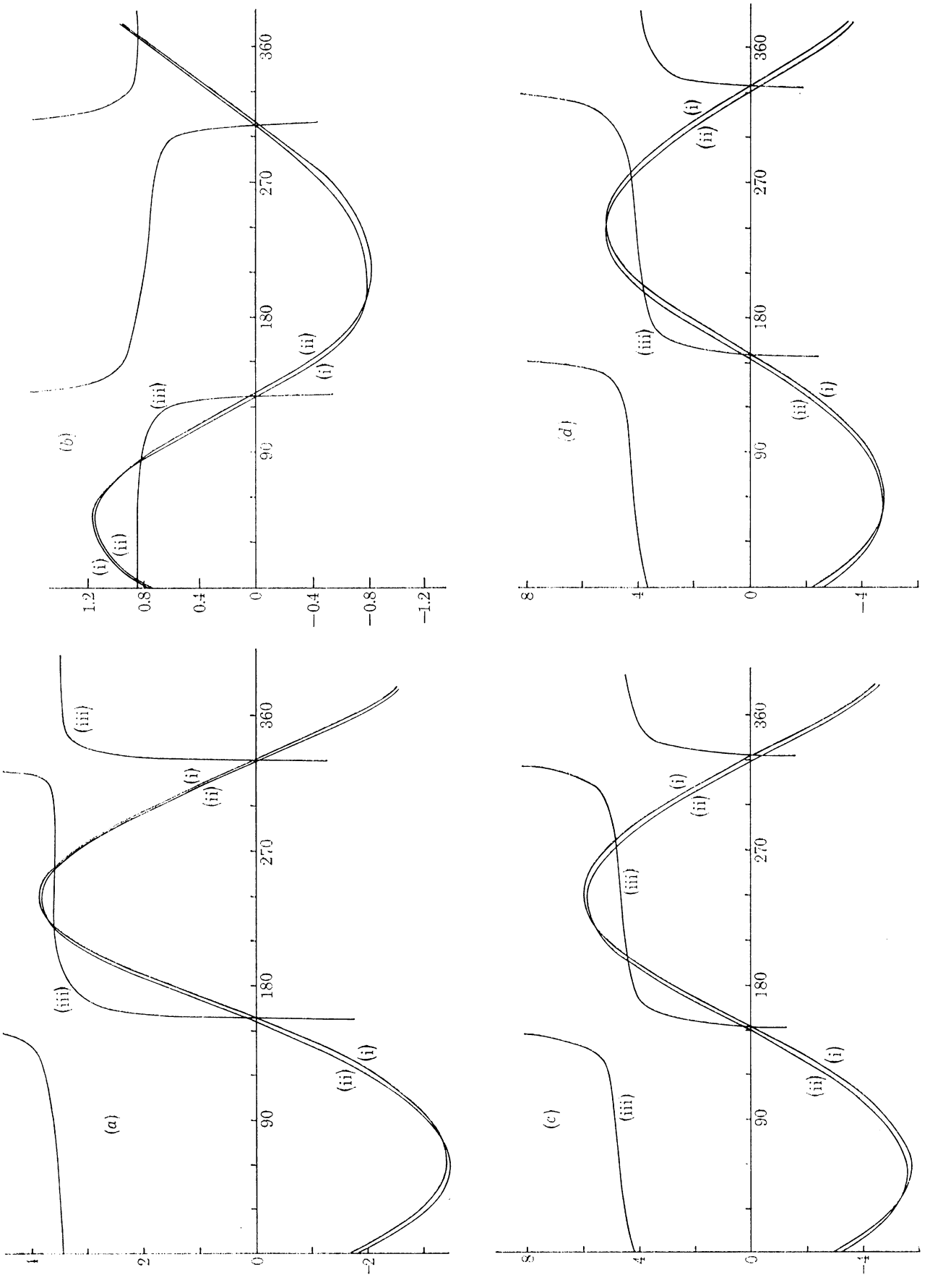

FIGURE 13. For description see opposite.

PHILOSOPHICAL TRANSACTIONS OF THE ROYAL SOCIETY A MATHEMATICAL, PHYSICAL & ENGINEERING SCIENCES

Banks also produced an analysis of the velocities in terms of the mean value U_n, V_n, and for each harmonic the phase ϕ_n, ψ_n and amplitude u_n, v_n of the velocity in the easterly and northerly directions respectively at each grid square n. Then if the virtual current is a_n in the easterly and b_n in the northerly direction, the theoretical mean cable voltage will be

$$k \sum_{n=1}^{N} (a_n V_n - b_n U_n),$$

N being the total number of sea squares for the given cable and k the product of magnetic field and the length of a grid square side. The amplitude of a given harmonic of cable voltage will be

$$k\left\{\left[\sum_{n=1}^{N} (a_n v_n \cos\psi_n - b_n u_n \cos\phi_n)\right]^2 + \left[\sum_{n=1}^{N} (a_n v_n \sin\psi_n - b_n u_n \sin\phi_n)\right]^2\right\}^{\frac{1}{2}}$$

and its phase

$$\arctan\left\{\frac{\sum_{n=1}^{N} (a_n v_n \sin\psi_n - b_n u_n \sin\phi_n)}{\sum_{n=1}^{N} (a_n v_n \cos\psi_n - b_n u_n \cos\phi_n)}\right\}.$$

These operations were performed, and the resulting amplitude and phase of cable voltage and volume transport are shown in figure 14 and table 3. The complex cable response is plotted in figure 15 and listed in table 3. The M_2 response is very close to that obtained from Mungall's M_2 velocity distribution in § 9. However, the harmonics have a calibration ratio which differs from M_2 by up to 25 %, either greater or less, and phase lags which differ from the M_2 lag by significant angles. M_4, the largest of the higher harmonics, differs considerably from M_2 in its response at each of the cables.

What is also important is the response of the cables to the mean velocity component. It is up to 20 % different to the M_2 amplitude ratio for all but the Anglesey–Isle of Man cable, for which the response to mean flow bears no relation to the M_2 calibration, being in fact negative. Inspection of the mean velocity for this cable shows that there is a local distribution of velocity resulting in a net flow across the cable section which is very small and in the opposite direction to the general trend, this latter being what influences the cable voltage. This is just the sort of velocity distribution which can render the cable results meaningless. Any empirical evidence that such a wide discrepancy exists between the the calibration for M_2 flow and for mean flow, is usually masked by the practice of assuming that any unexpected mean voltage levels can be explained in terms of a voltage zero error due to permanent earth-generated currents and an electro-chemical potential effect between the earth and the cable. Undoubtedly such a zero error does exist, but the above

FIGURE 13. Response of cables to a velocity distribution of M_2 and nonlinearly generated harmonics, over a tidal cycle.

(*a*) Cemaes Bay–Castletown. (i) Actual volume transport, one unit is 10^6 m^3 s^{-1}. (ii) Cable-predicted volume transport, using M_2 calibration, one unit is 10^6 m^3 s^{-1}. (iii) Instantaneous calibration, one unit is 4.55×10^5 m^3 s^{-1} V^{-1}.

(*b*) Port Erin–Ballyhornan. (i) Actual volume transport 10^6 m^3 s^{-1}. (ii) Cable-predicted volume transport, using M_2 calibration, one unit is 10^6 m^3 s^{-1}. (iii) Instantaneous calibration, one unit is 2.27×10^6 m^3 s^{-1} V^{-1}.

(*c*) Nevyn–Howth. (i) Actual volume transport, one unit is 10^6 m^3 s^{-1}. (ii) Cable-predicted volume transport, using M_2 calibration, one unit is 10^6 m^3 s^{-1}. (iii) Instantaneous calibration, one unit is 4.55×10^5 m^3 s^{-1} V^{-1}.

(*d*) Holyhead–Dublin. (i) Actual volume transport, one unit is 10^6 m^{-3} s^{-1}. (ii) Cable predicted volume transport, using M_2 calibration, one unit is 10^6 m^3 s^{-1}. (iii) Instantaneous calibration, one unit is 4.55×10^5 m^3 s^{-1} V^{-1}.

PHILOSOPHICAL TRANSACTIONS OF THE ROYAL SOCIETY A MATHEMATICAL, PHYSICAL & ENGINEERING SCIENCES

results suggest that it may not always be as easily calculated as is normally done by subtracting from the measured mean voltage the estimated mean flow multiplied by the M_2 calibration ratio.

In general, it can be said that for the higher harmonics, and in most cases for the mean flow also, the response does not differ so widely from the M_2 response as to seriously impair the analysis of cable data. However, the above results do demonstrate that the response does vary with frequency, and if very accurate analyses of data are required, corrections must be made accordingly to the standard method of applying a simple calibration factor to all frequencies.

TABLE 3. IRISH SEA CABLE RESPONSES TO M_2 + HARMONICS
(VELOCITY DISTRIBUTION FROM BANKS'S IRISH SEA MODEL)

		transport		signal voltage			phase lag (signal behind transport)
		amplitude	phase	amplitude	phase	amplitude ratio	
cable	harmonic	10^6 m^3 s^{-1}	rad	V	rad	10^6 m^3 s^{-1} V^{-1}	rad
Anglesey–Isle of Man	mean	0.00033	—	−0.0046	—	−0.072	—
	M_2	3.625	0.84	2.225	0.81	1.63	0.02
	M_4	0.260	1.38	0.1262	1.41	2.06	−0.02
	M_6	0.078	1.05	0.0444	0.97	1.75	0.08
	M_8	0.010	0.43	0.0056	0.32	1.81	0.11
	M_{10}	0.005	0.34	0.0022	0.42	2.14	−0.08
Port Erin–Ballyhornan	mean	0.0775	—	0.0352	—	2.20	—
	M_2	0.967	0.39	0.519	0.44	1.86	−0.04
	M_4	0.129	1.51	0.0554	1.49	2.33	0.01
	M_6	0.0159	−0.13	0.0072	−0.18	2.21	0.04
	M_8	0.0118	−1.40	0.0055	−1.39	2.19	0.0
	M_{10}	0.00085	0.52	0.0003	0.05	2.54	0.47
Nevyn–Howth	mean	0.0764	—	0.0294	—	2.60	—
	M_2	5.874	0.80	2.780	0.74	2.12	0.05
	M_4	0.0788	−0.85	0.0483	−1.01	1.63	0.15
	M_6	0.0919	0.42	0.0464	0.22	1.98	0.19
	M_8	0.0035	0.44	0.0022	0.0	1.57	0.43
	M_{10}	0.00265	−0.59	0.0011	−1.25	2.50	0.66
Holyhead–Dublin	mean	0.052	—	0.0262	—	1.98	—
	M_2	5.017	0.85	2.684	0.78	1.87	0.06
	M_4	0.138	−1.37	0.0932	−1.50	1.48	0.13
	M_6	0.092	0.53	0.0520	0.41	1.77	0.11
	M_8	0.0061	−0.53	0.0036	−0.77	1.70	0.24
	M_{10}	0.0053	−0.14	0.0024	−0.23	2.16	0.08

It must be pointed out, though, that these particular response curves should not be taken necessarily to be the true curves for the cables in question for two reasons (*a*) the velocity distribution which was used was the result of a dynamical model which had not been completely optimized regarding choice of friction coefficient, etc., and which was not fully checked against observations for the higher harmonics, (*b*) the harmonics involved were simply those generated from non-linear operations on an M_2 input. In reality there would be many other input frequencies and meteorologically driven motions, which would increase the number of important frequencies present and possibly change the flow pattern of the frequencies analysed above, particularly the mean flow distribution, with consequent alterations to the response curve. When dynamical model results containing a true spectrum of frequencies are available, a true theoretical response

PHILOSOPHICAL TRANSACTIONS OF THE ROYAL SOCIETY A MATHEMATICAL, PHYSICAL & ENGINEERING SCIENCES

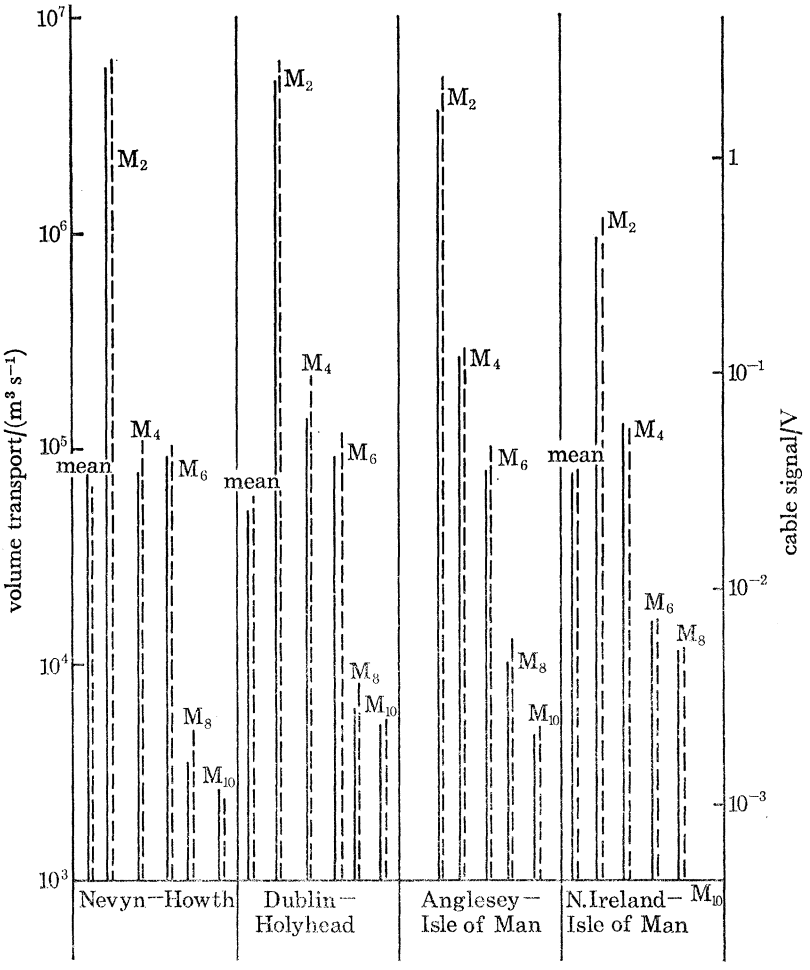

FIGURE 14. Comparison of amplitudes of separate harmonics of volume transport and voltage signal for the Irish Sea cables, using Banks's velocity distribution. ——, Volume transport; – – – –, voltage signal.

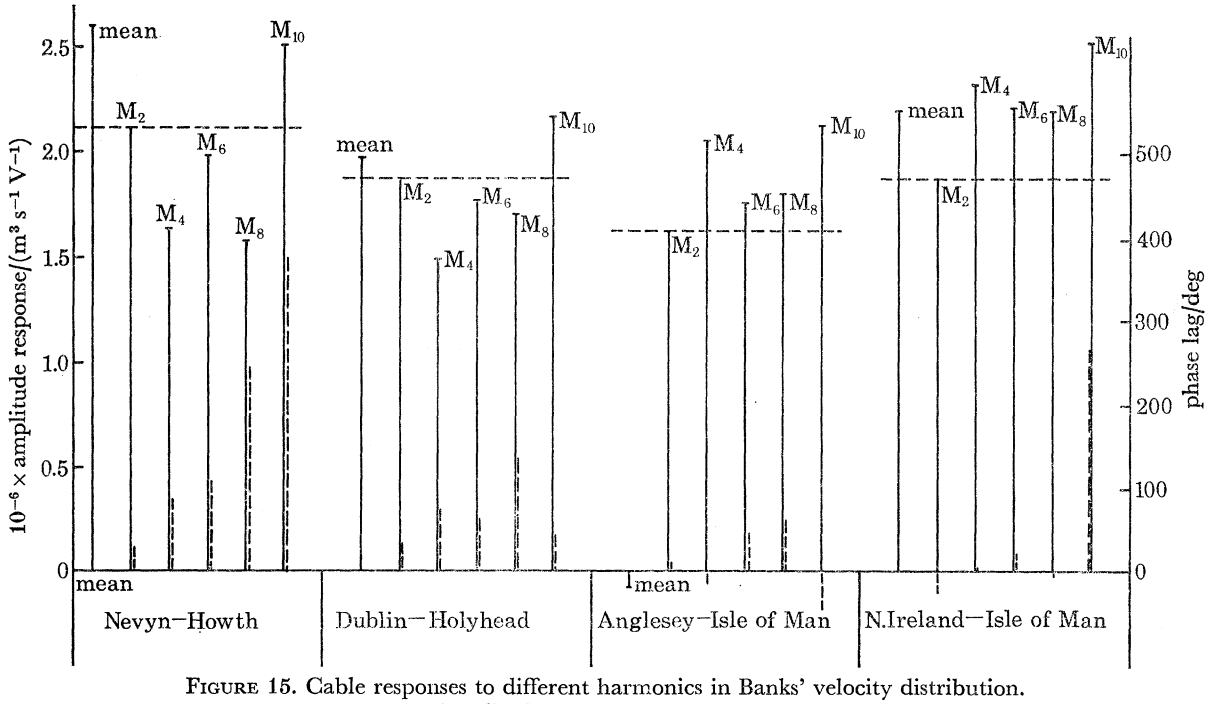

FIGURE 15. Cable responses to different harmonics in Banks' velocity distribution. ——, Amplitude response; – – – –, phase lag.

curve can be constructed. It will be particularly interesting to discover the response of the diurnal tidal species, the detailed response of the individual frequencies within each species, and from these whether the frequency response is a smooth curve or not.

12. The cable response to non-tidal motions

One important possible use of cable voltages is the monitoring of storm surges for input into real-time dynamical models. Bowden & Hughes (1961) have used cable residuals as a measure of non-tidal flow in the Irish Sea, relating it to wind stresses. Heaps (1975) is using cable residuals as a check on dynamical models of authentic storm surges. Once again, however, it is the M_2 tidal velocities which are used to calibrate the cable for interpretation of the voltage residuals in terms of volume flows. It is therefore important that typical storm surge flow patterns should be applied to the present method to enable comparison to be made between the actual flows and those predicted by tidally calibrated voltages.

The Irish Sea cables with parameters as defined in § 9 were used again, because suitable velocity distributions were available for that area. In particular the output from Heaps' dynamical Irish Sea model was used, with that model applied to two particular circumstances.

(*a*) *Ideal wind-driven circulation*

The velocity distributions used here were two hypothetical wind-driven circulation patterns, the result of applying a uniform southerly, or a uniform westerly wind to the whole of the Irish Sea, as described in Heaps (1974). When starting transients have damped out of the dynamical model, the depth mean steady state circulation, as applied to the cable models, is that illustrated in figure 16*a*, *b*. The resulting cable voltages, and the volume transports evaluated from them using the calibration factors derived in § 9, are compared with the actual volume transports in table 4. Included there are the results of applying the wind-driven circulation to the Cemaes Bay–Castletown cable for all four seasons. This completes the analysis of § 10, and demonstrates in fact

Table 4. Irish Sea cable responses to wind-driven circulation

cable	month	wind direction	transport $10^3 m^3 s^{-1}$	predicted voltage V	calibration for wind-driven flow $10^6 m^3 s^{-1} V^{-1}$	M_2 calibration $10^6 m^3 s^{-1} V^{-1}$	transport predicted by M_2 calibration $10^3 m^3 s^{-1}$
Cemaes Bay–Castletown	August	south	347.95	5.26	0.0661	1.63	8570
		west	−69.09	0.455	−0.152	1.63	741
	November	south	347.95	5.26	0.0661	1.65	8690
		west	−69.09	0.455	−0.152	1.65	751
	February	south	347.95	5.25	0.0662	1.68	8850
		west	−69.09	0.456	−0.1515	1.68	767
	May	south	347.95	5.26	0.0662	1.67	8790
		west	−69.09	0.455	−0.1518	1.67	760
Port Erin–Ballyhornan	August	south	98.132	−1.915	−0.0512	1.86	−3560
		west	67.881	0.484	0.142	1.86	900
Nevyn–Howth	August	south	401.37	−1.253	−0.320	2.08	−2610
		west	−6.76	2.93	−0.0023	2.08	6090
Holyhead–Dublin	August	south	370.15	−3.00	−0.123	1.87	−5610
		west	−11.13	2.64	−0.0028	1.87	4940

that the effect on the voltage output of the pattern of virtual current varying with seasonal conductivity changes is very small for this particular cable.

However, overall it is clear that the cable predictions and the actual volume transport bear no obvious relation to one another for any of the cables. The conculsion must be drawn that the cables are useless in measuring such a flow. The reason is apparent from figure 16. The velocity is very non-uniform across a cable section. For instance in figure 16*a*, between North Wales and Eire there are strong currents at the coast and a reverse flow in the centre of the channel, the worst sort of velocity distribution for a cable to measure. Around the Isle of Man the flow is confused, and there is no clear trend of velocity direction which will dominate the integration over space which governs the voltage measured by the cable.

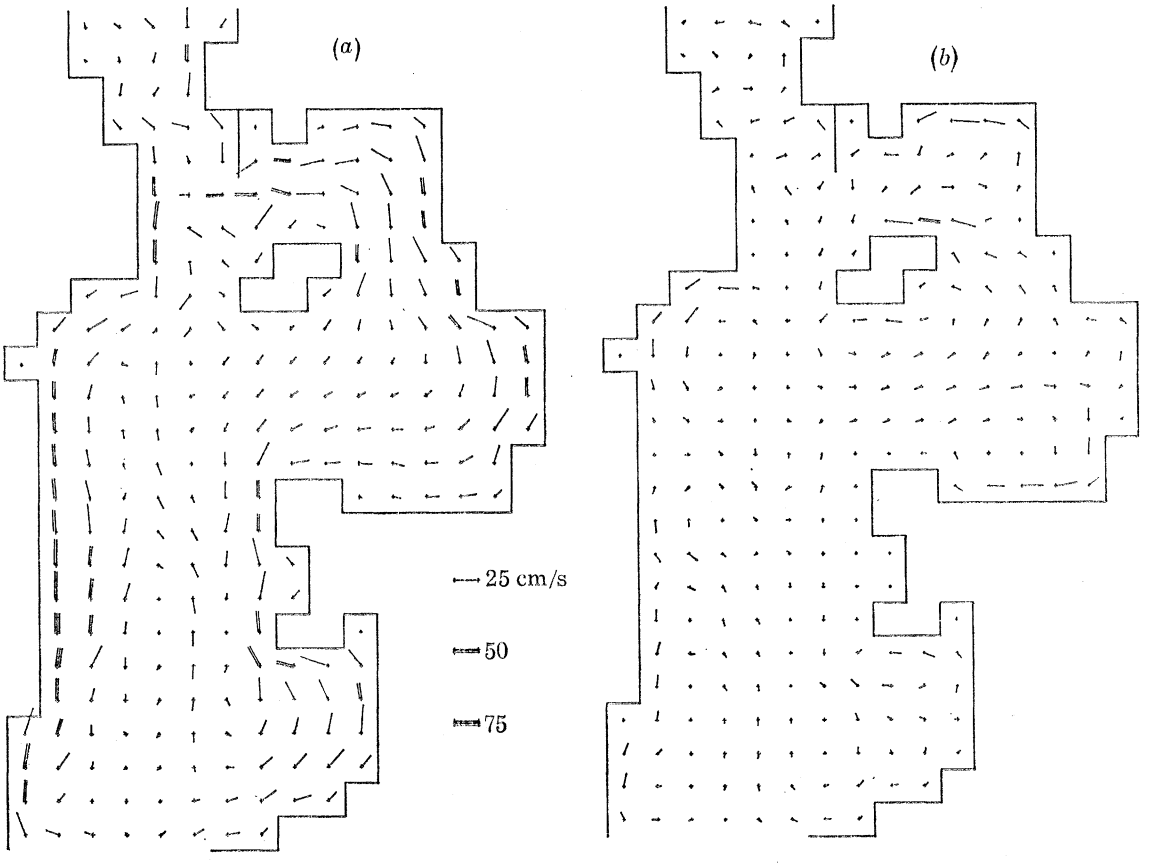

FIGURE 16. Depth-mean currents due to a uniform wind operating on Heaps' Irish Sea model. (*a*) South wind. (*b*) West wind.

Now these two velocity distributions are hypothetical, but it is quite possible that they represent to some extent the true velocity distribution of wind-driven residual flows resulting from a southerly or westerly wind prevailing for a number of days. Add to this the fact that in a true record there will be tidal residuals present, with a cable response governed in the way described in § 11, as well as d.c. earth currents and electrochemical potentials, and the use of long period residuals from cable voltages is seen to be very questionable.

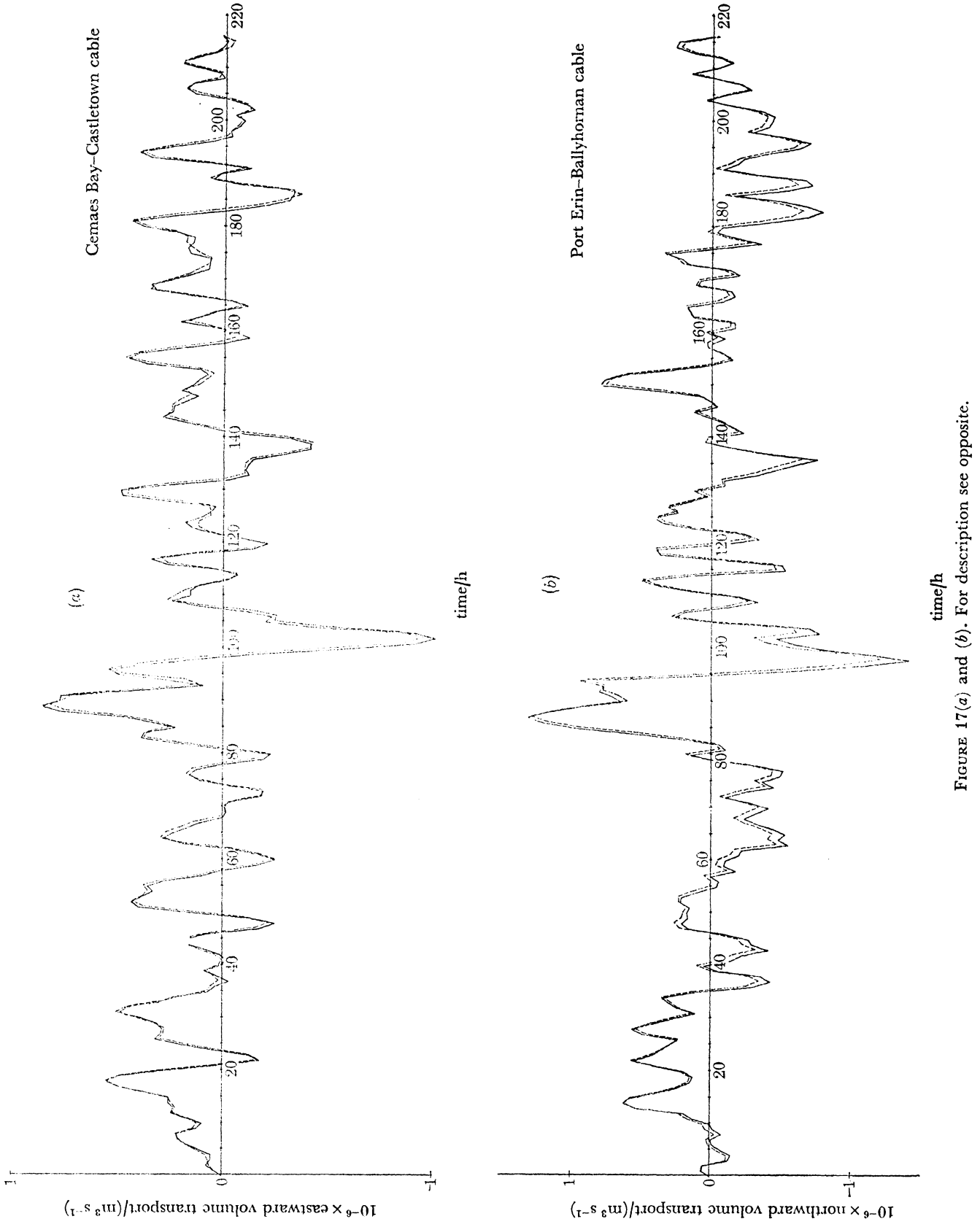

FIGURE 17(*a*) and (*b*). For description see opposite.

PHILOSOPHICAL TRANSACTIONS OF THE ROYAL SOCIETY A MATHEMATICAL, PHYSICAL & ENGINEERING SCIENCES

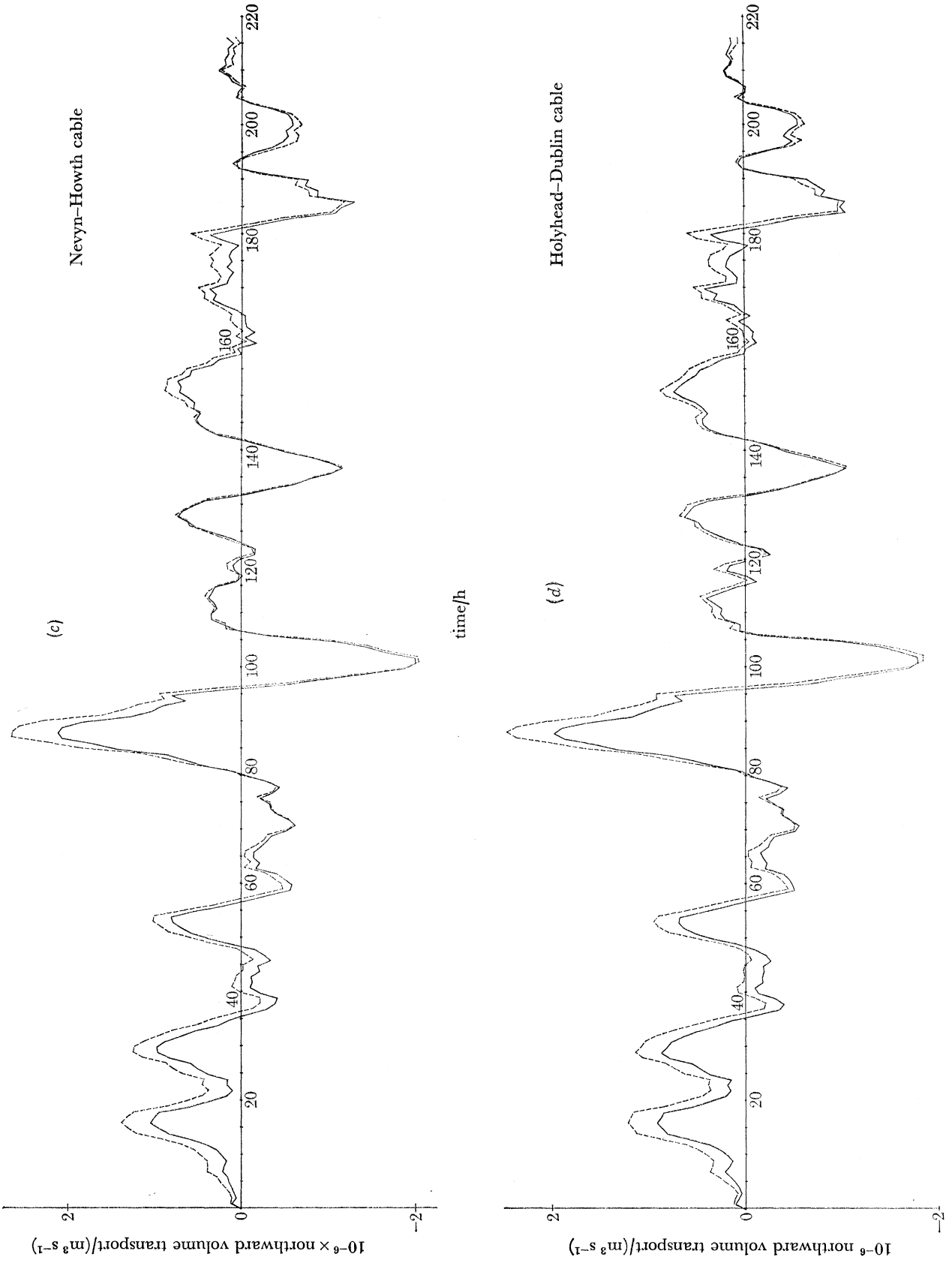

FIGURE 17. Comparison of actual (——) and cable predicted (– – –) volume transports during a storm surge period in the Irish Sea.

PHILOSOPHICAL TRANSACTIONS OF THE ROYAL SOCIETY A MATHEMATICAL, PHYSICAL & ENGINEERING SCIENCES

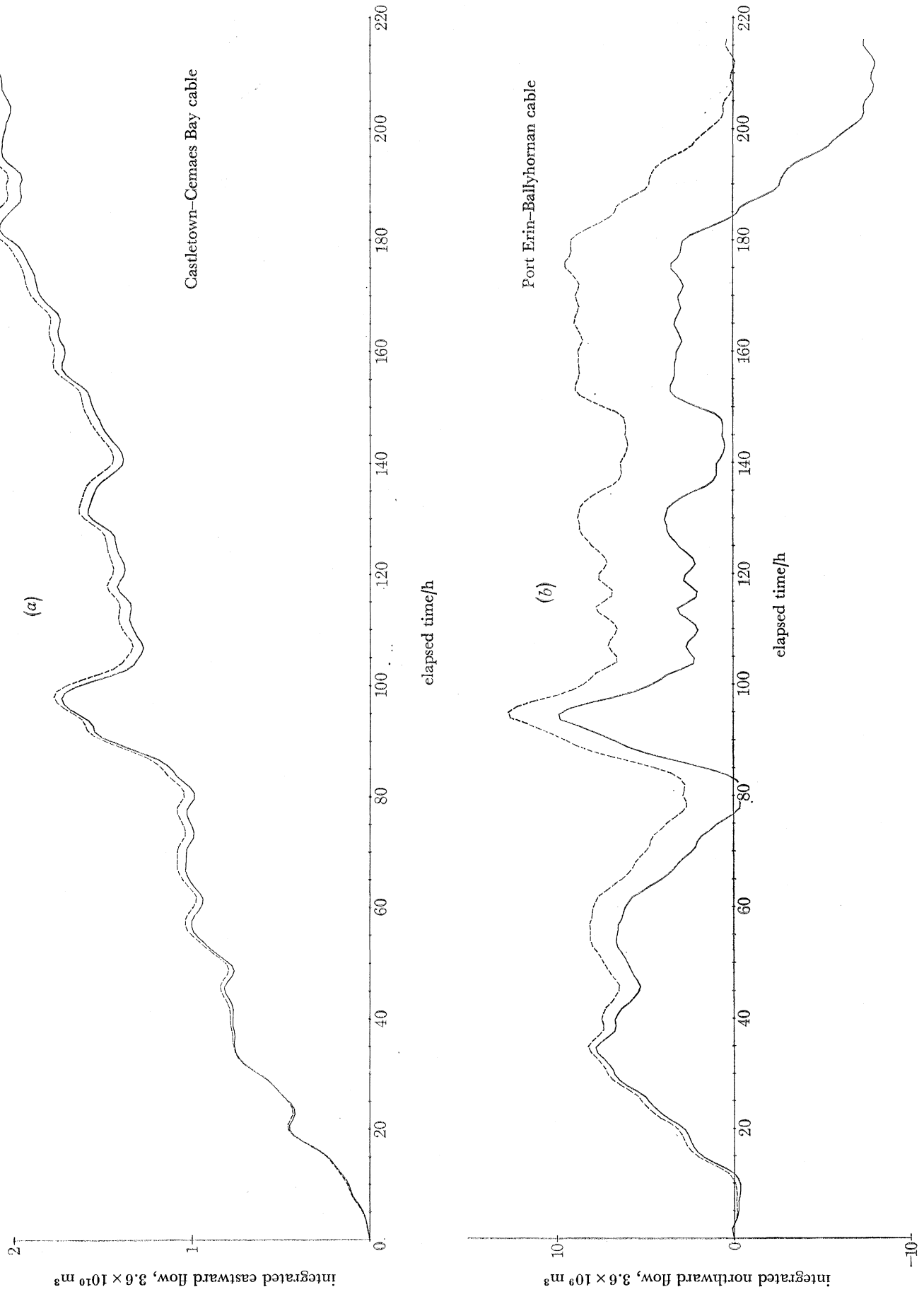

FIGURE 18(*a*) and (*b*). For description see opposite.

PHILOSOPHICAL TRANSACTIONS OF THE ROYAL SOCIETY A MATHEMATICAL, PHYSICAL & ENGINEERING SCIENCES

PHILOSOPHICAL TRANSACTIONS OF THE ROYAL SOCIETY A MATHEMATICAL, PHYSICAL & ENGINEERING SCIENCES

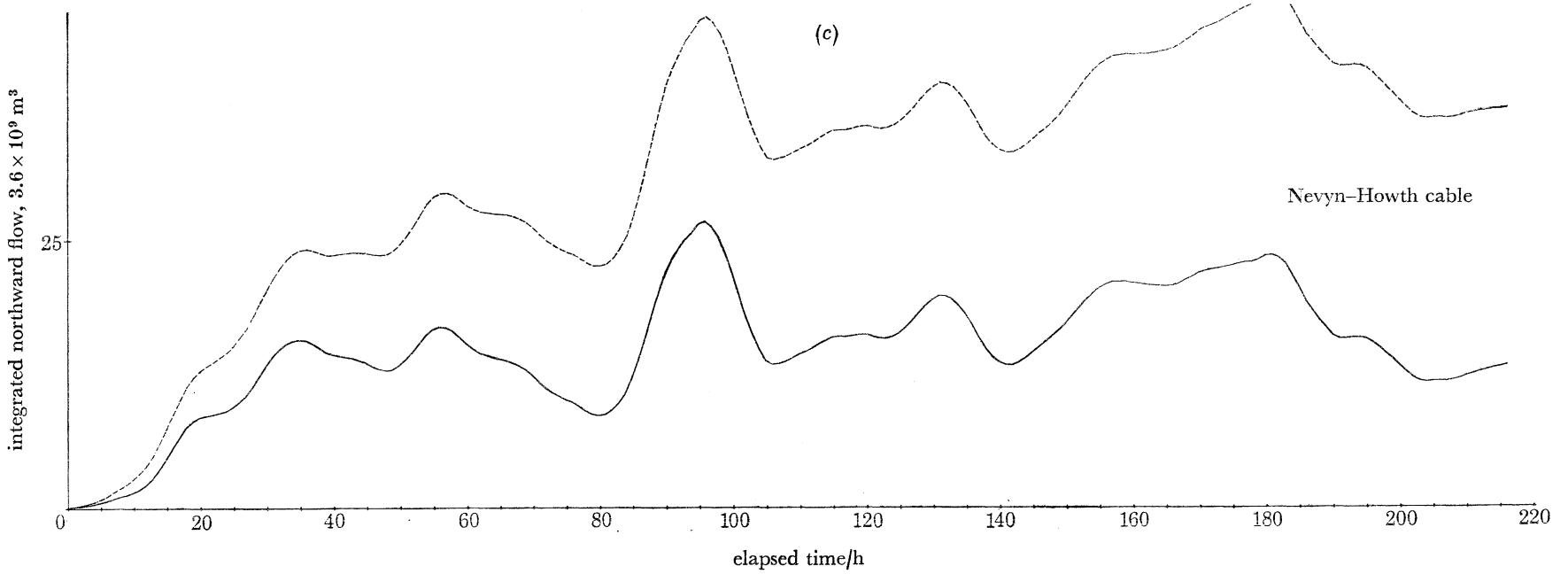

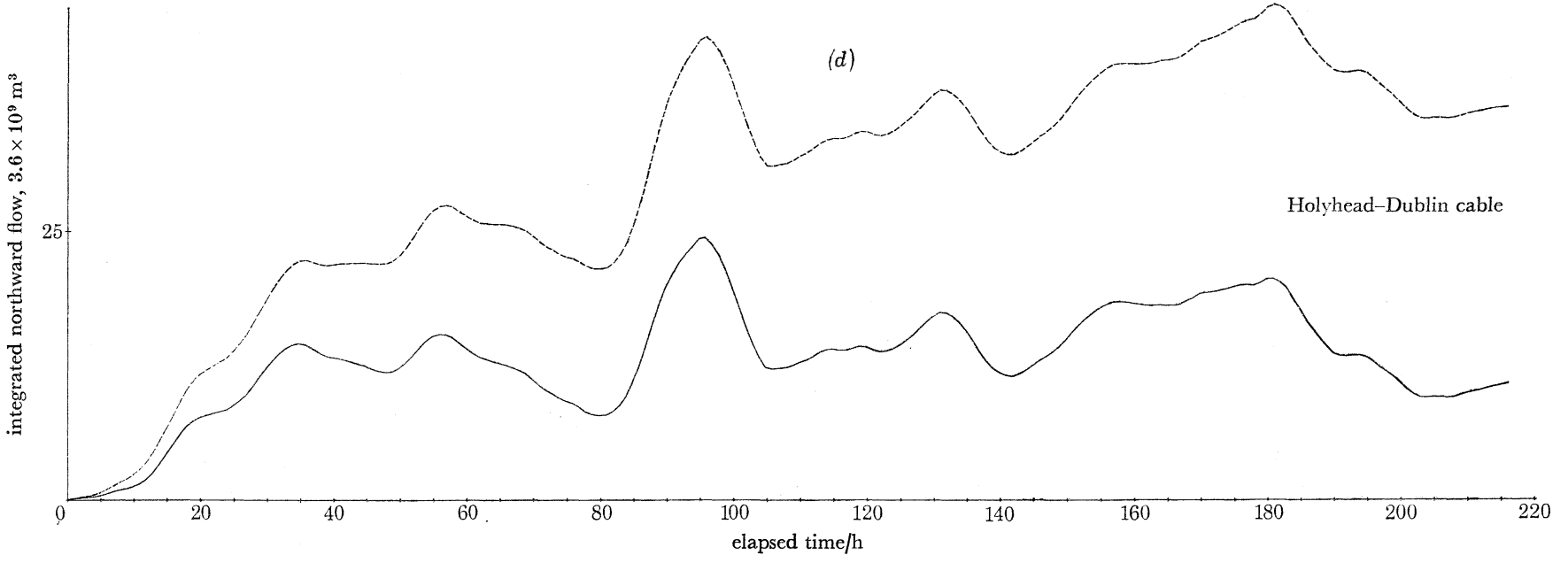

FIGURE 18. Time integrated volume transport during a storm surge period in the Irish Sea.
——, Actual; – – –, cable predicted.

(*b*) *Authentic storm surge residuals*

Residuals which fluctuate with a period of up to a couple of days can be separated from the record to eliminate the effect of zero errors due to earth currents and electrochemical potentials. The non-tidal flows due to storm surges come into this category, and for strong storms the surge shows up well in the cable voltage record. To usefully model the cable response to this phenomenon, which is neither a steady state situation nor recognizable as a sum of harmonics, it is necessary to supply to our model a velocity distribution which represents an actual storm surge situation which has occurred in nature. Fortunately Heaps has developed his dynamical model of the Irish Sea to an extent where it will realistically model an actual surge period which occurred between 00h00, 10 Jan. 1965, and 00h00, 19 Jan. 1965 (Heaps 1975). Depth mean currents for the whole of the Irish Sea, calculated by his model, were available for each of 217 consecutive hours, and so the cable voltages on the four cables were calculated at each hour. Once again the tidal calibration of § 9 was applied to the voltages to produce the cable-predicted volume transports across cable sections, for comparison with the true volume transports (i.e. as calculated directly from Heaps' model results). This comparison is plotted in figure 17*a–d*.

Agreement in this case is seen to be reasonably good. The general shape of the volume transport time series is followed closely by the cable prediction. The two Isle of Man cables are particularly good, but the major peak at 88 h is over-estimated on the Eire–N. Wales cables by a factor of 20 %. Moreover, although the general shape is quite good, these cables tend to predict a flow with a greater northward component of flow, irrespective of the actual flow direction (i.e. the predicted curve is shifted above the actual curve). This cannot simply be attributed to an over-estimation of the tidal calibrations, since that would lead to a high production of southerly flow when the flow was southwards, which is the opposite of the case most of the time. Since this will lead to an over-estimation of the net flow northwards, and since a similar but smaller effect was detected in the Isle of Man cable results, the two curves in figure 17 were integrated over time, to produce figures 18*a–d*. These represent the net volume of water which has flowed across the section since hour 0 at any given time. Apart from the Isle of Man–Anglesey cable, which shows a close correlation between cable predictions and actual flow, the other cables give results which are completely erroneous – even to the extent of being in the wrong direction if a suitable time is chosen to compare the actual and the predicted values. However, such an integration procedure is equivalent to using the cable to measure long period residuals and mean drifts, and this result is in concurrence with the conclusions reached above that the use of cables for such measurements is questionable.

However, this analysis does give confidence about using the cable voltages to describe the hour by hour fluctuations of residual volume transport (provided the tidal responses of the cable are known accurately enough for all the tidal frequencies to be satisfactorily subtracted from the record). This could then be used as input to dynamical models, provided long period integrations are not required. Care must none the less be taken in the cases where the peaks do not match. Of course, faced with a cable record there is no indication of which peaks match reality and which do not, but a clue to which parts of the record may be less reliable can be gained from looking at the flow pattern of depth mean velocity at hour 88 – the hour of the main peak (figure 19). A strong coastal flow, with lower flow in mid-channel has developed between Eire and North Wales, and it is this which must be producing the error in the two cables passing close to it. For the other two cables the flow pattern is much more uniform and the accuracy

correspondingly better. As a general rule, then, it could be inferred that when the surge flow pattern is regular and similar to the tidal flow pattern throughout the region influencing a cable, the surge results from that cable, calibrated tidally, may be considered reliable, but when the flow pattern is irregular, containing a gyre, reverse flows, or large coast-following current streams in an otherwise regular velocity field, then errors should be suspected in the cable results.

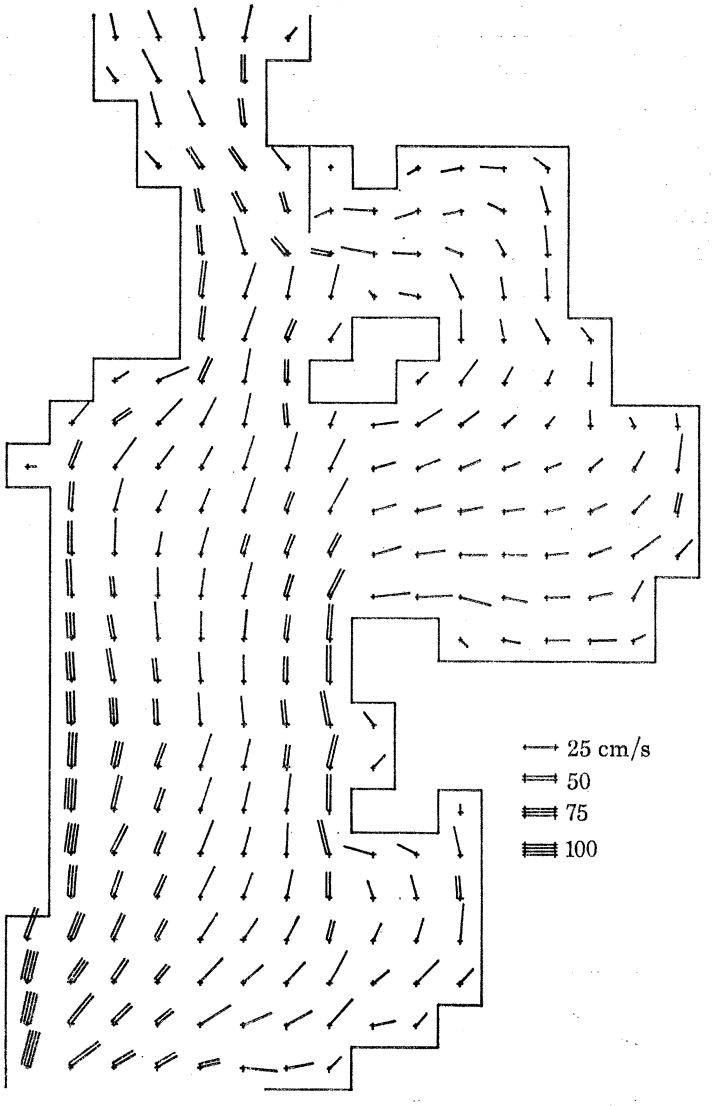

FIGURE 19. Storm surge velocity distribution at hour 88.

13. THE EFFECT OF A SIGNIFICANTLY LARGE TIDAL RANGE ON THE DOVER CABLE CALIBRATION

The Dover cable, spanning the English Channel from St Margaret's Bay to Sangatte, has been used several times to study the flow of water through the Straits of Dover, e.g. Bowden (1956), Cartwright (1961), Cartwright & Crease (1963). Allowance has been made, when calibrating it, for the variation of sea conductivity with season, but in every case, as for the Irish Sea cables, the

PHILOSOPHICAL TRANSACTIONS OF THE ROYAL SOCIETY A MATHEMATICAL, PHYSICAL & ENGINEERING SCIENCES

calibration based on the M_2 tidal flow has been used to evaluate mean volume transports from the mean voltage, after corrections for permanent earth currents and electro-chemical potentials.

Now in the Dover Straits, the tidal range is up to 8 m at spring tides, and the average mean depth is less than 30 m. Consequently, during a tidal cycle the virtual current distribution which defines the cable response to flow may vary considerably. At high tide a greater proportion of virtual current passes through the sea and less through the sea bed than at low tide. As in the consideration of seasonally varying conductivity in § 10, the magnitude of the effect increases with increasing earth conductivity. The influence on the voltage signal is to reduce it at low tide and increase it at high tide for the same depth mean velocity distribution, i.e. the voltage signal is modulated over a tidal cycle. Of course the volume transport through the Straits is also modulated in a similar way, being the product of depth and depth mean velocity. However, there is no certainty that the voltage will be modulated by tidal rise and fall in exactly the same way as the volume transport, and it is valuable to know exactly what the response of the cable sensitivity is to tidal rise and fall. It is particularly important to discover if the mean value of voltage (modulation is likely to introduce a non zero-mean voltage even with an input of pure M_2 velocities) is related to the mean value of volume transport by the calibration factor based on the M_2 signal, because this could well affect the use of the mean value of voltage in calculating surface slopes for levelling purposes, as well as the calculation of residual drifts through the Straits.

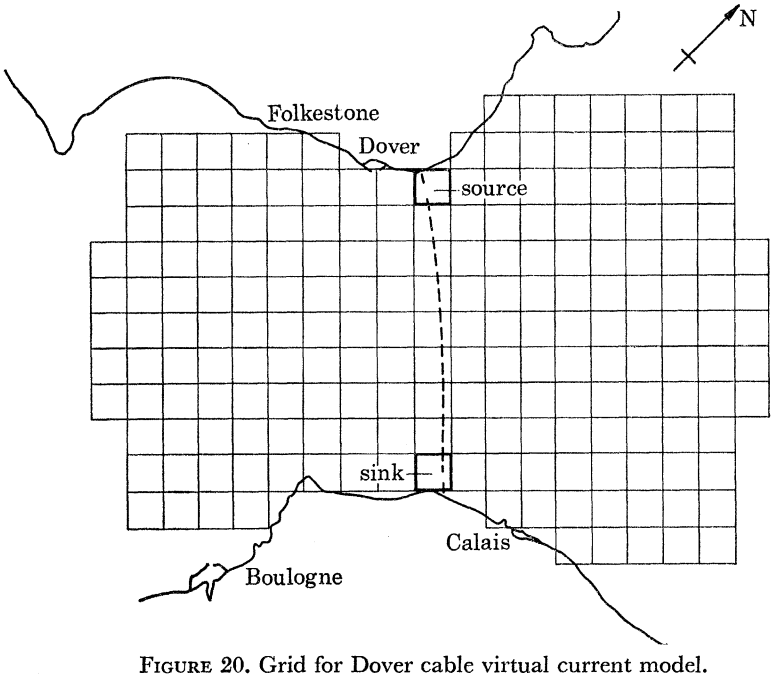

FIGURE 20. Grid for Dover cable virtual current model.

The model shown in figure 20 was therefore constructed to calculate the virtual current distribution corresponding to the Dover cable. The depths were taken from the Admiralty charts, and the conductivity used was that given for August by the temperature and salinity distributions in the North Sea atlas of C.P.I. pour l'Exploration de la mer (1962). Information on the phase and amplitude of tidal elevation was also supplied for each grid square from the German tidal atlas (Marineobservatorium Wilhelmshaven 1942), the amplitude being supplied as (M_2+S_2), (M_2-S_2) and M_2 to correspond respectively to springs, neaps and midcycle tidal conditions. The

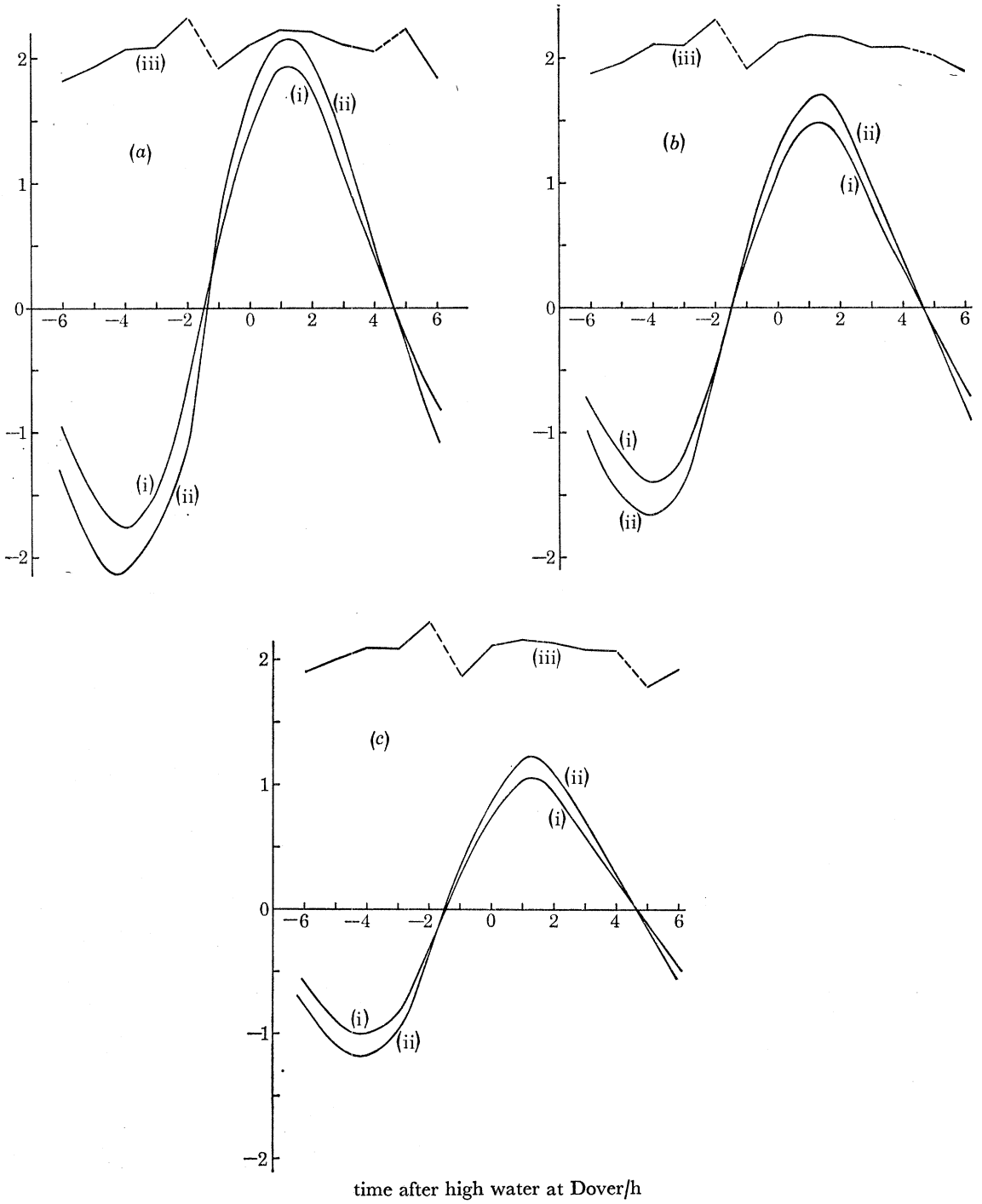

FIGURE 21. Volume transport, theoretical voltage and instantaneous calibration of Dover cable over a tidal cycle. Curve (i) volume transport, one unit is 10^6 m^3 s^{-1}; (ii) voltage signal, one unit is 0.88 V; (iii) instantaneous calibration, one unit is 4.55×10^5 m^3 s^{-1} V^{-1}. (*a*) Spring tide; (*b*) at the middle of the fortnightly cycle; (*c*) neap tide.

phase was taken as that of M_2 in each case. For each case the virtual current distribution was calculated for 13 different times during the tidal cycle, i.e. six-hourly values before and after high water at Dover. The general points that emerge from inspection of the virtual current results are that a greater proportion of the virtual current passes through the sea at high water, as expected, and also that at high water the distribution is altered so that proportionately more weight is given to the upstream and downstream squares, and those squares near the line of the cable in fact have an absolutely less weighting at high tide than at low tide.

In the absence of self-consistent values of depth mean currents from a numerical model, hourly values of current were obtained from the Admiralty (1963) Tidal Stream Atlas. These are surface values, but were taken as depth mean currents. Any adjustment to convert them into a better representation of depth mean currents, e.g. by Van Veen's formula, would merely involve scaling by a constant factor which does not influence the calculation of cable sensitivity. Because these currents are not necessarily an accurate representation of the true current distribution and may not conform to continuity conditions, not too much attention must be paid to the absolute values of voltage and volume transport which are deduced from them. However, they can provide an illustration of whether volume transport and voltage are modulated in the same way, i.e. even if the volume transports as calculated are not realistic, the voltage signal should be capable of predicting such transports if the cable is to be considered reliable.

Figure 21 shows the curves of volume transport calculated directly from the velocity and the voltage signal calculated by the virtual current method, over 13-hourly values of a tidal cycle. The volume transport in this case was calculated at each hour from the product of the local tidal stream and the local depth as obtained by adding the instantaneous tidal elevation to the mean chart depth in each grid square, summing over the column of grid squares joining the cable ends. The instantaneous calibration factor is also plotted, but does not follow the typical shape of a single harmonic as in § 9, because of the extra harmonics and mean value which are obviously present. The cable voltage clearly predicts well the volume transport for the basic M_2 constituent, but from figure 21 it is not clear whether the other harmonics and mean value have a similar response. Therefore the 13-hourly values of voltage and transport were subjected to harmonic analysis by a least squares method (using the Bidston tidal analysis algorithm), to extract the mean value and amplitude and phase of the M_2, M_4, M_6, M_8 and M_{10} tidal constituents. The results are shown in figure 22. As was noted above, the actual shape of figure 22 may owe as much to the inadequacies of the current data input as to the true physics of the situation, i.e. some of the higher harmonics may have been present in the input velocity data and not be due solely to the modulation effect as intended. However, the cable response curves obtained from these results should be a reasonable estimate of the true response of the cable under conditions of tidal rise and fall being significantly large. Figure 23 and table 5 show the cable response as calculated by dividing the volume transport of each harmonic in figure 22 by the corresponding voltage.

Now it is the amplitude of M_2 which is the calibration factor used by those analysing Dover cable data. In our case this has a value of $1.0 \times 10^6\,m^3\,s^{-1}V^{-1}$. This is low compared with empiri- calibrations, e.g. Bowden (1956) gives a figure of 8.0 $mV\,cm^{-1}\,s^{-1}$ for depth mean current in August 1953, which, using the cross-sectional area of $1.22\,cm^2$ quoted by Cartwright (1961) (somewhat larger than that calculated from the mean depths in our model), would result in a transport calibration of $1.53 \times 10^6\,m^3\,s^{-1}\,V^{-1}$. Cartwright's result is $1.65 \times 10^6\,m^3\,s^{-1}\,V^{-1}$, but this is for May observations, and if it is scaled by the ratio Bowden gives between May and August calibrations it is reduced to $1.52 \times 10^6\,m^3\,s^{-1}\,V^{-1}$. The discrepancy here can probably be credited

partly to the inaccuracy of using an earth conductivity of 9.7×10^{-3} S m^{-1}, itself obtained from Bowden's analysis using Longuet-Higgins' formula. For more accurate analysis of the cable response, from dynamical model generated current values, it would be necessary to adjust σ_E to give better agreement with empirical calibration for M_2. Since at present, however, we are concerned simply to look at the broad effects of modulation due to tidal rise and fall, and the theoretical M_2 calibration is just 30 % less than the empirical value, then it is believed that the response curve of figure 23 has some relevance to the real cable situation.

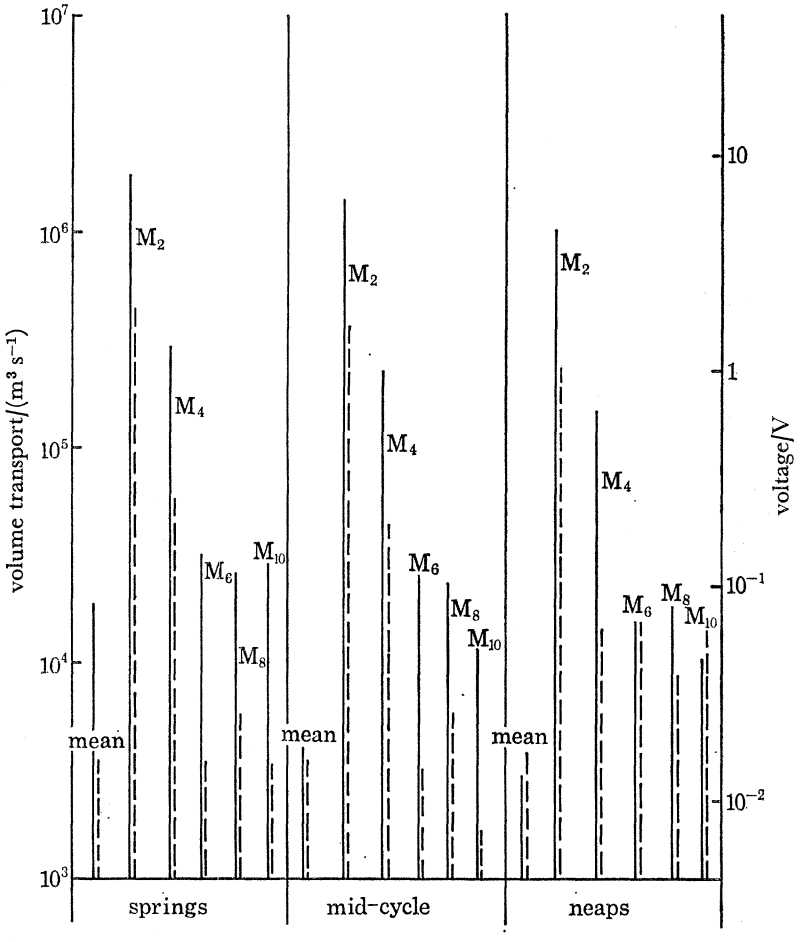

FIGURE 22. Amplitudes of volume transport (——) and voltage (– – –) from harmonic analysis of Dover cable results. N.B.: mean value of voltage and amplitude are of opposite sign.

From figure 23 it is clear that the M_2 response has very little phase lag, and its amplitude varies only 4 % between springs and neaps, although this 4 % variation could influence the separation of M_2 and S_2 over a fortnight. However, the response of the other harmonics differs considerably from that of M_2, e.g. the M_4 amplitude ratio is 25 % greater than for M_2 at springs and midcycle, and over 100 % greater at neaps. The other harmonics up to M_{10} give amplitude ratios differing even more from M_2, and also differing widely between springs and neaps, with attendant variations of phase lag between volume transport and signal. While M_6, M_8 and M_{10} are of small absolute magnitude, and might well be lost in the noise of a true signal, the M_4 contribution is significant. Without a pure M_2 velocity input to the exercise, it cannot be concluded that the frequency variation of sensitivity is due only to the modulation by tidal rise and fall. Some of the

variation is probably due to the spatial distribution of the higher harmonics in the input data. None the less it is certainly evident that to deduce the M_4 transport from the M_4 voltage signal using the M_2 calibration factor could lead to serious errors.

Of even greater importance is the relation between the mean transport over a tidal cycle and the mean cable voltage. For springs and midcycle, the mean volume transport is from SW to NE

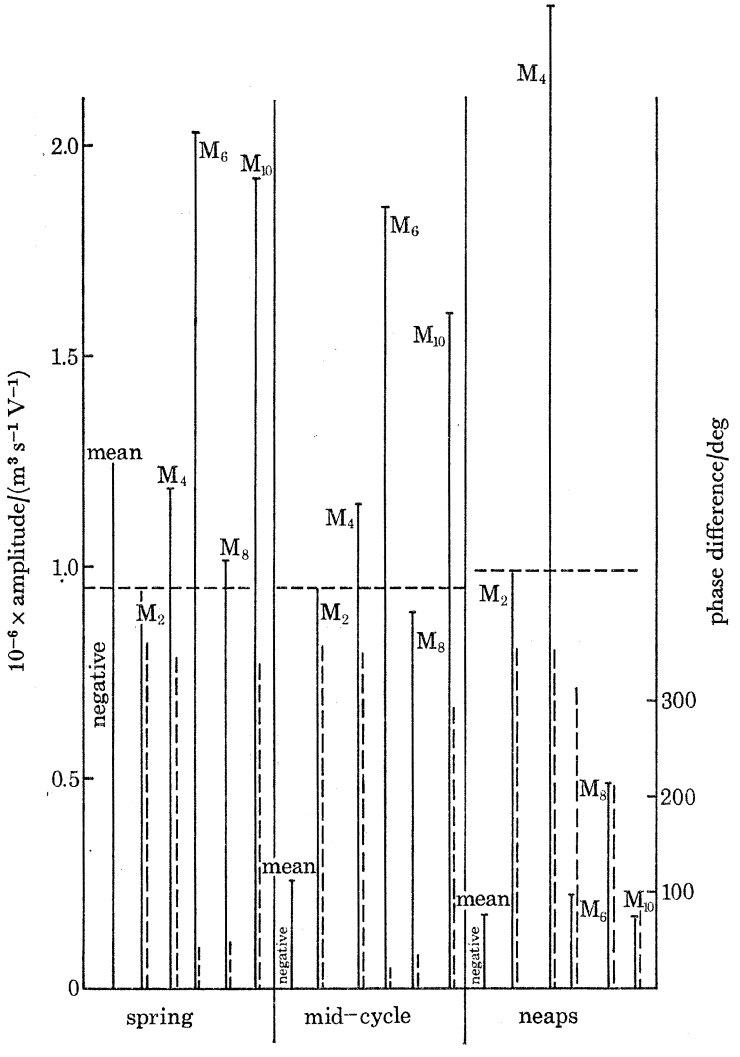

FIGURE 23. Response of Dover cable. ——, Amplitude ratio; – – –, phase difference.

TABLE 5. DOVER CABLE RESPONSES

	springs		midcycle		neaps	
harmonic	amplitude ratio 10^6 m^{3}s^{-1}V^{-1}	phase lag deg	amplitude ratio 10^6 m^{3}s^{-1}V^{-1}	phase lag deg	amplitude ratio 10^6 m^{3}s^{-1}V^{-1}	phase lag deg
mean	−1.24	—	−0.260	—	−0.178	—
M_2	0.95	−0.9	0.95	−1.0	0.99	−3.9
M_4	1.18	−13.9	1.15	−9.5	2.33	−5.9
M_6	2.03	41.4	1.86	22.1	0.227	−48.0
M_8	1.02	48.6	0.89	35.8	0.485	−149.4
M_{10}	1.93	−20.0	1.60	−67.7	0.165	84.2

and for neaps it is reversed, whereas for each case the flow predicted from the mean of the cable voltage, using the M_2 calibration, is in the opposite direction, and bears no relation in magnitude to the transport it is supposed to represent. Interpreting this result in a simple levelling exercise (ignoring the fact that the level depends on the integral of depth mean current across the section which may differ from the flux of water as predicted by the cable voltage), the error involved is one of up to 3 cm/s in depth mean velocity, corresponding to a levelling error of 1.0 cm according to Cartwright & Crease. This is 9 % of the contribution by the true residual current through the Straits of Dover, and is the same size as the wind stress correction to Cartwright & Crease's levelling exercise.

It is not claimed that these errors necessarily exist in the cable data used by Cartwright & Crease, since they are based on a crude velocity input. But only the modulating effect of tidal rise and fall has been considered so far. If true tidal residual flows, and meteorologically driven flows were tested in this model, and similar results to § 10 and §11 were obtained, then the use of the cable to measure mean flows through the Straits would certainly be extremely suspect. Without better current data input, it is not worth while to probe further in this direction. However, when a detailed dynamical model of the area is available, it will be vital, if confidence is to be placed in results from the Dover cable, for a complete range of typical tide and surge conditions to be applied to the cable model. The above results confirm that tidal rise and fall have a significant effect on the results, and must be included in the model. For the levelling application, close attention must be paid to the mean values, and it would be interesting to attempt to relate the voltage mean not only to the volume transport mean, but also to the time mean of the depth mean current, since it is in fact this latter which contributes to the surface slope. It is in cases where the tidal range is large compared with the depth that mean current and mean transport can differ greatly, even in direction, and it may be that the mean cable voltage gives a better representation of the former than the latter, which would be a help to the hydrodynamic leveller. Meanwhile, until such ideas are tested, the theoretical results so far urge caution in the use of the broad assumption that the M_2 calibration of the cable can be applied to all other flows through the Dover Straits.

14. Conclusions

At the beginning of this paper, various questions were raised regarding the accuracy of using submarine cables as oceanographic flowmeters, in particular whether the calibration remains constant with time. The theoretical method of calculating the expected voltage from a given velocity distribution, using the virtual current approach for calculating a weighting vector, produces results for the basic semi-diurnal tidal calibration which compare quite well with empirical calibrations. Seasonal variation of calibration can also be modelled well, if care is taken to choose a suitable earth conductivity. Therefore, even though the uncertainty of choosing the correct earth conductivity prevents a completely reliable estimate of the calibration factor from being made without empirical measurements, it is believed that the method presented does model accurately the variation of response of the cable voltage to different flow distributions.

The instantaneous calibration of the cables seems to vary considerably with time for every sort of oceanographic flow. However, much of this can be attributed to a phase shift between the volume transport and the voltage signal. Rather than look for variations of calibration with time, except due to seasonal variations of conductivity, it is more helpful to consider the frequency response of the cable, with M_2 as the dominant harmonic which gives the equivalent of the

empirical calibration. It is then found that the higher harmonics, because they have a different velocity distribution, do have a different response which must be taken into account when analysing voltage data. No investigations were made into cable responses to diurnal tidal motions, but it was found that storm surge flows with periods up to about a day were fairly accurately monitored by the cable, except when the velocity distribution was not the same sort of pattern as the tidal flow but contained a gyre or reverse flow in the vicinity of the cable. Long period residuals and mean flows were not monitored well by the cable. Where tidal range was large compared with the depth, further errors were introduced to the cable measurement of mean flow and harmonics higher than the semi-diurnal frequency.

It is suggested that where cable results are required to be accurate, use should be made where possible of the results of dynamical models covering the whole spectrum of tidal frequencies to enable the true frequency response of the cable to tidal flows to be calculated. Where cable voltages are being used to monitor storm surges, particularly as input to predictive dynamical models, checks should be made of the surge flow pattern to make sure that it is regular. For periods when it is not, then either the cable results should be discarded, or else the instantaneous calibration could be calculated in the manner described by this paper and applied to the residual cable voltage instead of the M_2 calibration. Where mean flows are required from the cable voltages, a model should always be constructed to account for all the causes of a mean voltage signal (e.g. mean flows due to nonlinear operations on tidal frequencies, wind-driven flows, and modulation of the signal by tidal rise and fall) to see if the voltage can be meaningfully correlated to the volume flow.

References

Admiralty 1963 Hydrographic Department. *Dover Strait, tidal stream atlas*. NP. 233.

Bevir, M. K. 1970 The theory of induced voltage electromagnetic flowmeters. *J. Fluid Mech.* **43**, 577–590.

Bialek, E. L. 1966 *Handbook of oceanographic tables*. Washington, D.C.: U.S. Naval Oceanographic Office.

Bowden, K. F. 1955 Physical oceanography of the Irish Sea. *Fishery Invest., Lond.*, ser. II, **18**, 1–67.

Bowden, K. F. 1956 The flow of water through the Straits of Dover related to wind and differences in sea level. *Phil. Trans. R. Soc. Lond.* A **248**, 517–551.

Bowden, K. F. & Hughes, P. 1961 The flow of water through the Irish Sea and its relation to wind. *Geophys. J. R. astr. Soc.* **5**, 265–291.

Cartwright, D. E. 1961 A study of currents in the Strait of Dover. *J. Inst. Navig.* **14**, 130–151.

Cartwright, D. E. & Crease, J. 1963 A comparison of the geodetic reference levels of England and France by means of the sea surface. *Proc. R. Soc. Lond.* A **273**, 558–580.

Conseil Permanent International pour l'Exploration de la Mer 1962 *Mean monthly temperature and salinity of the surface layer of the North Sea and adjacent waters from 1905 to 1954*. Denmark: Charlottenlund Slot.

Heaps, N. S. 1974 Development of a three-dimensional model of the Irish Sea. Symposium on the physical processes responsible for the dispersal of pollutants in the sea, with special reference to the near-shore zone. Aarhus, 1972. *Rapp. P.-v. Réun. Cons. perm. int. Explor. Mer.* **167**, 147–162.

Heaps, N. S. & Jones, J. E. 1975 Storm surge computations for the Irish Sea using a three-dimensional numerical model. *Mem. Soc. r. sci. Liège*, ser. 6, **7**, 289–333.

Hughes, P. 1969 Submarine cable measurements of tidal currents in the Irish Sea. *Limnol. Oceangr.* **14**, 269–278.

Longuet-Higgins, M. S. 1949 The electrical and magnetic effects of tidal streams. *Mon. Not. R. astr. Soc. geophys. Suppl.* **5**, 285–307.

Longuet-Higgins, M. S., Stern, M. E. & Stommel, H. 1954 The electrical field induced by ocean currents and waves, with applications to the method of towed electrodes. *Pap. phys. Oceanogr. Met.* **13**, no. 1, 37 pp.

Marineobservatorium Wilhelmshaven, Hamburg 1942 Karten der harmonischen Gezeitenkonstanten für das Gebiet des Kanal. Ausgabe (*a*), 1803.

Mungall, J. C. H. 1973 Numerical tidal models with unequal grid-spacing. Ph.D. dissertation, University of Alaska Institute of Marine Science.

Shercliff, J. A. 1962 *The theory of electromagnetic flow measurement*. Cambridge University Press.

Shercliff, J. A. 1965 *A textbook of magnetohydrodynamics*. Oxford: Pergamon Press.

Wertheim, G. K. 1954 Studies of the electric potential between Key West, Florida, and Havana, Cuba. *Trans. Am. geophys. Un.* **35**, 872–882.

PHILOSOPHICAL TRANSACTIONS OF THE ROYAL SOCIETY A MATHEMATICAL, PHYSICAL & ENGINEERING SCIENCES